5-kW Xenon Ion Thruster Lifetest

Michael J. Patterson
National Aeronautics and Space Administration
Lewis Research Center
Cleveland, Ohio

and

Timothy R. Verhey
Sverdrup Technology, Inc.
Lewis Research Center Group
Brook Park, Ohio

NASA

5kW XENON ION THRUSTER LIFETEST

Michael J. Patterson
National Aeronautics and Space Administration
Lewis Research Center
Cleveland, Ohio 44135

Timothy R. Verhey
Sverdrup Technology, Inc.
Lewis Research Center Group
Brook Park, Ohio 44142

Abstract

This paper describes the results of the first lifetest of a high power ring-cusp ion thruster. A 30-cm laboratory model thruster was operated steady-state at a nominal beam power of 5kW on xenon propellant for approximately 900 hours. This test was conducted to identify life-limiting erosion mechanisms and thruster design modifications, and to demonstrate operation using simplified power processing. The results from this test are described including the conclusions derived from extensive post-test analyses of the thruster. Modifications to the thruster and ground support equipment, which have been incorporated to solve problems identified by the lifetest, are also described.

Introduction

The objective of the high power ion thruster program at NASA Lewis Research Center (LeRC) is to define the requirements for 5 and 10kW engineering model inert gas ion thrusters. The motivation is to insure the capability to rapidly proceed into a flight program in response to national mission requirements. Several critical prerequisites for proceeding into an engineering model stage for either 5 or 10kW thrusters must first be met, including:

(1) definition, design, fabrication and performance characterization of a laboratory model thruster, compatible with mission performance requirements
(2) verification of the life potential of the laboratory model thruster
(3) definition of power-processor interface requirements, and
(4) establishment of protocols and procedures to maximize repeatability and transportability of results

A considerable database has been established for ion thruster performance on inert gas propellants[1-3]. Although there is adequate information to glean preliminary design criteria for laboratory model 5kW and 10kW xenon ion thrusters, there is insufficient data to address thruster lifetimes at these power levels. The limited lifetime data on inert gas ion thrusters includes a 4300 hour test of a 25-cm ring-cusp xenon ion thruster at 1.3kW[4], and a 567 hour test of a 30-cm divergent field xenon ion thruster at 10kW[5]. The former lifetest was conducted at a low power level as the thruster was developed for north-south stationkeeping applications and subsequent tests have indicated that the thruster thermal design precludes its operation in the 5-to-10kW power range[6]. The latter lifetest identified internal erosion rates so severe in the divergent-field design as to terminate further efforts on this type thruster at NASA-LeRC.

This paper describes the results obtained from the 900 hour lifetest of a laboratory model 30-cm diameter ring-cusp ion thruster operating on xenon propellant at 5kW beam power. The purpose of the lifetest, the first extended-duration test of a high power ring-cusp ion thruster, was to identify the life potential of, and any required design modifications to, the laboratory model thruster. This represents the initial effort to establish a 10,000 hour capability of a 5kW ion thruster. These lifetime and power-level targets are consistent with projected near-term Earth-space mission requirements[7-9].

The lifetest was the completion of an initial experimental phase which included defining thruster and lifetest performance targets; designing a thruster to satisfy the performance targets (selection of beam area, magnetic circuit, materials, etc.); and conducting a variety of pre-lifetest experiments. Those experiments included performance characterization on xenon propellant over an input power range of 1.5-to-10kW, developing cathode activation

procedures, demonstrating rapid-start to full-power operation, and conducting several extended-duration tests at 5kW to verify the thruster (component design) and the operation of the ground support equipment (including the data acquisition, thruster autonomous shut-down, and vacuum facility systems). These efforts are described in the paper.

At the conclusion of the 900 hour test, extensive thruster post-test analyses were conducted and the results and conclusions of these analyses are presented. Modifications to the thruster, and to the ground support equipment which have been incorporated to solve problems identified by the lifetest are also discussed.

Hardware Description

This section describes the experimental and ground support hardware used for the lifetest.

Thruster

The laboratory model xenon ion thruster, developed for performance and extended-duration testing, is shown in Figures 1a and 1b. The overall operational goals for the ion thruster are shown in Table I and include the capability of reliable operation for 10 khr at 5 kW, in a specific impulse range of 3800 to 4000 seconds, thrust levels of 0.18-0.20 N and efficiencies in the range of 67 to 78 percent.

The laboratory model thruster depicted in Figure 1 can be described according to its major components, which include: the discharge chamber, the discharge cathode assembly, the ion optics, and the neutralizer assembly. Details of the design and construction of each of these components are listed in Table II, and are discussed in the following sections.

discharge chamber - The discharge chamber (Figure 1) is composed of several parts (all at anode potential during operation) including: a 3-piece exterior shell with magnets, anode spacer ring, welded anode, and a main plenum, as well as ceramic insulators for mounting the thruster to the test stand, and mounting the ion optics to the discharge chamber. The exterior shell is fabricated from 0.15-cm thick mild steel, and includes a disk backplate, a cylinder (nominal O.D. of 34.6-cm and length of 24.6-cm), and a polepiece ring. Attached to the interior surfaces of the backplate, cylinder, and polepiece are a total of 3 rings of samarium-cobalt (molar ratio of 2:17) permanent magnets arranged in rings of alternating polarity so as to form a cusp-field. The anode spacer ring, fabricated from aluminum, is secured to the interior of the shell backplate, and mechanically bolts the anode to the exterior shell to insure concentricity of the anode-to-shell cylinder and to control the anode surface-to-magnet surface gap. The anode is fabricated of 0.23-cm thick grit-blasted aluminum. It forms the pressure vessel and site of electron current collection for the

plasma discharge. The primary sites for current collection are 3 lines directly above the magnet rings, at the magnetic-cusps. The main plenum consists of 0.64-cm diameter stainless steel tubing formed into a 24.5-cm diameter ring, which is mounted onto the interior backwall of the anode concentric with the chamber. The downstream surface of the plenum has 30 equally-spaced 0.03-cm diameter holes for injection of the main propellant flow into the anode chamber. A 0.64-cm diameter stainless steel tube is welded to the plenum, and penetrates through the rear of the exterior shell for attachment of the main propellant feed line. The propellant feed line consists of a 0.64-cm diameter fluoro-carbon elastomer tubing of approximately 1 m in length (for electrical isolation of the thruster) terminated on both ends with 0.32-cm diameter stainless steel tubing sections with A-N fittings.

discharge cathode assembly - The discharge cathode assembly includes the hollow cathode, cathode tube clamping fixture, starting electrode, and high temperature insulators (for electrical isolation of the cathode components from the anode-potential engine body). The cathode assembly was designed for operation without a cathode keeper. The hollow cathode consists of a 10.2-cm long, 0.64-cm diameter molybdenum-41-rhenium tube with a 2% thoriated-tungsten orifice plate electron-beam welded to one end of the tube. The orifice plate has a thickness of 0.13-cm, and width of 0.58-cm, with a centered 0.15-cm diameter electron-discharge-machined hole through the thickness dimension. The downstream surface of the orifice has a machined 90-degree chamfer which penetrates to a depth of 0.05-cm. Interior to the tube is a sintered porous tungsten cylinder impregnated with a 4:1:1 molar ratio of BaO-CaO-Al$_2$O$_3$. Exterior to the tube at the downstream end is a swaged heater consisting of 8 turns of a tantalum sheath-MgO-tantalum wire sandwich. The coiled heater is friction-fitted to the tube starting at approximately 0.32-cm upstream of the orifice plate. Exterior to the coiled heater is approximately 12 layers of untextured 0.013-mm thick tantalum foil wrapped and spot-welded to the exposed portions of the coil for heat-shielding. The heater is designed to raise the cathode tube temperature to 1100 degrees centigrade with approximately 100 watts power. The cathode tube, heater, and a starting electrode penetrate through the rear of the steel shell and anode chamber along the centerline of the thruster. The cathode tube clamping fixture is fabricated of stainless steel, and is mounted on the cathode insulator which is bolted to the rear backplate center of the steel discharge chamber shell. The clamp mechanically supports the cathode tube and starting electrode in the thruster, and permits axial adjustment of the cathode assembly in the anode chamber. It also provides an electrical pickup for cathode common

(negative side of the discharge supply) and for the cathode heater and starting electrode. At the upstream end of the cathode tube, a stainless steel and grafoil compression fitting provides a leak-tight propellant connection and transition to a fluoro-carbon elastomer tube which is connected to the cathode propellant feed line. The starting electrode consists of a ceramic-sheathed stainless steel wire of 0.11-cm diameter which runs parallel to the hollow cathode into the anode chamber. The tip of the electrode is exposed stainless bent at an angle and honed to a point to provide a high-voltage spark breakdown (across a 0.10-cm gap between the tip and orifice plate of the cathode) for discharge ignition.

ion optics - The ion optics used for the lifetest are of a 2-grid, small-hole-accelerator-grid (SHAG) geometry with a nominal diameter of 30-cm (effective beam diameter of 28.2-cm). Neither the screen nor accelerator grid had been tested prior to the lifetest. The nominal thickness of both electrodes is 0.36-mm. The aperture diameters for the screen and accelerator grids are 0.19-cm and 0.11-cm, respectively. The holes for both grids are arranged in a hexagonal array with an open-area-fraction of 0.67 for the screen grid and 0.24 for the accelerator grid. The grids were hydroformed simultaneously with a nominal dish depth at center of 2.5-cm. Both grids are mounted to NASA-LeRC designed and fabricated molybdenum mounting rings. Prior to the lifetest, the grids were aligned with the assistance of an optical comparator, and the grid-to-grid cold-gap was documented at 389 separate locations. The nominal grid gap at centerline is 0.76-mm.

neutralizer assembly - The neutralizer assembly consists of a hollow cathode, keeper, and keeper support assembly and shadow-shielded ceramic insulators. The neutralizer hollow cathode is similar to the discharge cathode described previously, except for the following modifications: the cathode tube is 6.35-cm in length, with a centered 0.05-cm diameter hole in the orifice plate; at the upstream end of the tube, a stainless steel swaged fitting is made to make a leak-tight propellant connection and transition to a 0.64-cm diameter stainless steel tube used for axially positioning the cathode with respect to the ion optics; at the end of the stainless steel tube, a transition is made to a fluoro-carbon elastomer tube which is connected to the neutralizer propellant feed line. The keeper consists of a molybdenum bar with a 0.47-cm diameter hole at one end, which is positioned 0.13-cm downstream of the cathode orifice plate, with the hole in the orifice plate and keeper bar aligned to form an 'open-keeper' geometry. At the opposite end of the keeper bar, a single-point mechanical and electrical attachment is made using a 0.26-cm minor diameter threaded stainless steel rod. The stainless rod runs parallel to the cathode tube, and is sheathed with a shadow-shielded ceramic insulator. The rod and keeper are mechanically attached to the front ground-screen plate which surrounds the thruster and shields the high potential surfaces of the thruster from the beam plasma. The neutralizer cathode is pointed downstream, and located at an axial position 8.9-cm downstream and 8.9-cm radially out from the outermost accelerator grid holes. The neutralizer assembly was the only major component not to undergo an optimization process (in its design or position with respect to the ion beam) prior to the lifetest.

Ground Support Equipment

The following sections describe the equipment and preparation necessary to initiate and conduct the lifetest.

power supplies, control system, and data acquisition- The thruster was operated using 60 Hz laboratory power supplies prior to and during the lifetest. Figure 2 shows an electrical schematic of the thruster and power supplies. As mentioned previously, the thruster was designed with simplified power processing requirements. The thruster requires only four power supplies for steady-state operation, including two high-voltage supplies (one each for the screen and accelerator grids), and two low-voltage supplies (one each for the main discharge and neutralizer keeper). In addition to these supplies, three other supplies are used to start the thruster. Two low-voltage heater supplies activate the discharge and neutralizer cathodes, and a high-voltage supply provides a pulse-breakdown to facilitate discharge cathode ignition.

The positive and negative high-voltage supplies for the screen and accelerator grids are motor driven, three phase, full wave bridge rectified units each with an open circuit output voltage capability of 2500 V. The overcurrent trip set-points of the screen and accelerator supplies were set at 8.0 A and 0.67 A, respectively. The output voltages of the two supplies are maintained constant (to within approximately +/- 50 V) through analog meter relays which close the loop on the primary power drive motors.

The main discharge supply consists of a direct current output power supply connected in series with a transistorized series pass current regulator. This system provided an open circuit voltage of 80 V and a maximum limited current of 40 A. The neutralizer keeper supply has a single phase, full wave rectified output, with an open circuit voltage of 380 V to facilitate ignition of the cathode. Both the discharge and neutralizer heater supplies, used to activate the low work function inserts in the hollow cathodes, produce alternating current with 10 A/20 V capability. A high-voltage supply (3kV/3 micro-second pulse) was also used to create a breakdown between the starting electrode and the discharge cathode to facilitate discharge ignition.

Prior to the lifetest all power supplies

3

and metering were calibrated on a load bank. The output voltage and current ripples of each supply were also quantified using an oscilloscope.

The control system includes the control-logic for dealing with a 'recycle', and the monitoring and control capability to operate the thruster in steady state in an unattended mode. A high-voltage thruster 'recycle' is initiated whenever an overcurrent is sensed on either the screen or accelerator grid supplies (due to an inter-grid arc, or other). At this point the power to both high voltage supplies is interrupted (removing the high voltage present on the thruster grids), and the supply outputs are grounded. Concurrently, the discharge current is commanded back from the run set-point (22.0 A at 5kW) to some reduced level (typically 8.0-to-12.0 A) to decrease the ion production rate in the discharge. At this point the power is restored to the high voltage supplies, and the voltage is reapplied to the thruster grids, with the accelerator grid voltage recovery leading that of the screen supply (to preclude electron backstreaming from the neutralizer to the screen grid). As the high-voltage supplies are restored to full running voltage the discharge current is increased to the original run set-point, and a beam is extracted. The release and recovery timing, and voltage and current set-points during a recycle 'event' are all tailored to the steady-state operating point of the thruster. Because the high-voltage power supplies used in this effort are motor-driven, a recycle (from beam-off to full beam-on) could last as long as 10 seconds.

The control system associated with the power supplies is also designed to permit steady state, unattended operation of the thruster. Several thruster parameters are monitored including beam, discharge, and accelerator grid impingement currents, and discharge and neutralizer keeper voltages. In the event any of these parameters are out-of-range for a specified time, the thruster is commanded off. The recycle frequency is also monitored, and in the event the frequency exceeds a pre-specified rate of greater than 10 in a 2 minute period, the thruster is commanded off. Further, the thruster control system is tied in series with the vacuum facility control system, so in the event of a facility failure the thruster is commanded off. None of the power supplies are operated under closed-loop-control on any thruster parameters.

Two eight-channel strip-chart recorders were used for data acquistion during the lifetest to continuously monitor all thruster/power supply system parameters (11 electrical and 3 propellant parameters), as well as the vacuum facility pressure.

propellant feed system - The propellant feed system provides a controlled flow of gaseous propellant to the thruster through three separate feed lines, one each for the main plenum, discharge and neutralizer cathodes. A schematic of the propellant feed system used during the lifetest is shown in Figure 3. At one end of the system are the propellant (high purity - 99.995 percent pure - research grade xenon) and purge gas (high purity - 99.999 percent pure - research grade argon) high pressure bottles. Downstream of the propellant bottle are two pressure regulators in series; relief, precision metering, and check- and cut-off valves; an in-line pressure gauge; filter; and mass flow transducers. All propellant feed system lines consist of either stainless steel (with A-N fittings) or fluoro-carbon elastomer tubing. The entire propellant feed system was both pressure and leak-checked after assembly, and prior to the initiation of the lifetest.

The propellant flow rate during all testing was operated 'open-loop'; that is, no mass flow controllers were integrated into the propellant feed system, so that all flow adjustment was done manually using precision metering valves. This approach was used because the authors are aware of no high-reliability commercial mass flow controllers presently available for the flow ranges of interest. Several different mass flow control devices have been tested in conjunction with ion thruster operation at NASA-LeRC. A variety of failure modes have been experienced with these devices, resulting in some instances in catastrophic damage to thruster components.

The use of two laboratory gas regulators in series in the propellant feed system was an attempt to insure a constant delivery pressure at the precision metering valves (hence, a constant mass flow rate into the thruster) under conditions where the propellant bottle pressure would drop by as much as an order-of-magnitude (such as extended-duration tests). The bottle regulator had maximum inlet and outlet pressures of 3000 psig and 200 psig respectively; the second regulator had maximum inlet and outlet pressures of 1000 psig and 30 psig respectively. At the initiation of the lifetest, the xenon propellant bottle pressure was approximately 800 psig, with the bottle and second regulator second-stages set at 95 psig and 22 psig respectively.

Considerable care was exercised to insure accurate propellant flow meter calibration prior to and after the lifetest. This involved using volumetric/displacement hardware integrated into the propellant feed system at the location of the ion thruster, and delivering xenon propellant at the working pressure through the feed lines (passing through the mass flow transducers). A correlation was then established between the indicated and true mass flow rates (at multiple flow conditions) for each of the propellant lines. A linear correlation coefficient of greater than 0.997 was obtained for each of the three lines.

vacuum test facility - The vacuum test facility used for the lifetest (shown schematically in Figure 4) is a horizontal

chamber 4.6-m in diameter by 19.2-m long located at NASA-LeRC. Twenty 0.8-m diameter oil diffusion pumps, with freon traps at about 242 K, were used to provide an initial no-load pressure of 6.7×10^{-5} Pa. The operational pressure (ionization gauge readings corrected for gas type) during the lifetest was approximately 1.7×10^{-3} Pa at a total xenon mass flow rate of 54.1 sccm. A quadrupole residual gas analyzer was used to identify and estimate the partial pressure of facility background gases in the 1-100 AMU range, some of which could react with thruster component surfaces and alter erosion rates.

To accomodate the lifetest, modifications to the facility and to facility operating procedures were made. A beam shield (see Figure 5) consisting of a graphite disk and approximately 17 sq. m of graflex (flexible graphite sheet) was installed to cover existing aluminum louvres located at the mid-tank position, 9.4-m from the thruster. The purpose of the shield was to reduce the amount of sputtered material coming back onto the thruster. All interior vacuum chamber surfaces were cleaned to remove diffusion pump oil residue, which could contaminate the thruster. Numerous glass slides were installed in the vacuum chamber to quantify the target back-sputtered efflux and diffusion pump oil back-streaming. Facility and thruster shut-down procedures were developed in the event of a refrigeration system malfunction (resulting in an increase in freon trap temperatures and release of volatiles), or failure of an oil diffusion pump heater (resulting in oil back-streaming into the vacuum chamber). A vacuum chamber purge system was installed so that in the event of a facility shut-down during thruster operation the chamber would be pressurized with high purity argon.

Pretest Thruster Documentation

This section describes thruster documentation efforts prior to the initiation of the lifetest.

Preliminary Experiments

Over a period of several months prior to the initiation of the lifetest, a variety of thruster and thruster component experiments were conducted to optimize and quantify the performance of the laboratory model thruster, and to develop procedures and protocols. These included: (1) selection of discharge and neutralizer cathode geometries based on emission current requirements and cathode temperature data, and definition of preliminary insert activation procedures on xenon propellant (discussed in Appendix A); (2) selection of magnet material type and vendor based on irreversible field-loss measurements obtained from a variety of rare-Earth magnet materials under steady-state and cyclic heating conditions; (3) performance characterization of the laboratory model thruster over an input power range of 1.5-to-10kW on xenon propellant; (4) tests to demonstrate rapid-

start to full-power operation of the thruster (the thruster was brought from discharge ignition to 5kW beam power in less than 240 seconds with zero high-voltage recycles); and (5) five extended-duration tests conducted at about 5kW to verify the operation of the data acquisition system, the unattended thruster shut-down system, and the design of some thruster components (results are described in Table III). These tests were conducted using a vacuum facility and propellant feed system other than that used for the lifetest. However results obtained immediately prior to the lifetest were found to be comparable to the thruster performance obtained during preliminary experiments.

Performance

Immediately prior to the initiation of the lifetest, performance data were recorded for the thruster operating with the pristine ion optics and discharge and neutralizer hollow cathodes. These data included: (1) discharge current-voltage characteristics (to define the discharge electrical and propellant efficiencies), taken at the target 5kW propellant flow rates; (2) neutralizer keeper and coupling voltages vs. neutralizer propellant mass flow rate, for various keeper currents; and (3) accelerator grid impingement current vs. total accelerating voltage, for various beam currents (to define the ion optics perveance). These data are compared to data obtained directly after the lifetest, all of which are presented in the 'Post Test Thruster Analyses' section.

Hardware

An extensive pre-lifetest documentation of the laboratory model thruster components was conducted to allow comparisons with their post-lifetest condition. Documentation of the lifetest ion optics included: (1) precision measurements of several hole geometries and diameters on both grids, using both machined-gauges and a photo-microscope; (2) precision thickness measurements (to within +/- 2.5 microns using a modified deep-anvil micrometer) of both grids at multiple locations; (3) precision mass measurements (to within +/- 0.002 gm) of both grids; (4) assembled grid-gap measurements (to within +/- 25 microns) along three grid diameters; and (5) photography of both grids at multiple locations. Pretest documentation of both discharge and neutralizer cathodes included: (1) precision measurements of the orifice plate dimensions using a photomicroscope; and (2) photography of the orifice plates and tubes. Discharge chamber documentation included magnetic field measurements at the magnet surfaces, anode surfaces, and in the discharge volume.

Prior to final assembly and documentation of the ion thruster, all major components underwent an ultrasonic cleaning process using acetone and alcohol. Final thruster assembly was conducted using essentially clean-room procedures. Prior to

5

installation of the thruster into the vacuum chamber, leakage resistance across thruster high-voltage surfaces and insulators was measured using a high voltage ohmmeter. This was done to verify the integrity of the thruster and to provide a database for comparison after the lifetest. Measurement of electrical resistance was also performed and recorded for both the discharge and neutralizer cathode heaters.

Immediately after final assembly of the thruster and prior to the initiation of the lifetest, tests were conducted to characterize the thruster performance. These tests included 16.0 hours of steady-state operation at 5kW, and 49.4 hours of operation at a variety of throttled conditions.

Test Results

This section discusses the events and results of an 890 hour lifetest of the 30-cm diameter laboratory model ring-cusp xenon ion thruster operating at an average beam power of 4.9kW (average input power of 5.5kW). First presented is a test chronology, followed by a review of the overall thruster performance and the performance of each major thruster component, and finally a discussion of the performance of the ground support equipment.

Chronology

Figure 6 shows a chronology of the lifetest. The lifetest was initiated on December 1, 1989 at 1600 hours EST and was terminated on January 8, 1990 at 1452 hours EST, after completion of 890.0 hours of run time over an elapsed period of 910.9 hours (an effective duty cycle of 97.7%). The remaining elapsed time of 20.9 hours was spent at beam-off or thruster-off conditions during seven test interruptions. During the 890.0 hours of run time, the thruster was at full power for 884.8 hours or 99.4% of the run time. The remaining 5.1 hours was spent at throttled conditions during 1889 high-voltage recycles.

All seven test interruptions (or 'events') during the lifetest identified in Figure 6 were either power supply failures or operational problems directly attributable to the power supplies. Event #1 occurred at 184.5 hours run time, when it was decided to turn off the thruster high voltage for 2 hours to permit examination of the screen and accelerator supplies. At approximately 150 hours run time the recycle frequency suddenly increased by approximately a factor of three (to 2.4 per hour), with no apparent thruster or facility change that could be identified as causal or contributory. At 166 hours one of six mercury arc tubes (used for voltage rectification) in the accelerator supply was observed to have a non-uniform discharge. This was interpreted as a possible sign of tube failure, which would result in an increase in the ripple on the output voltage of the power supply. Prior to the initiation of the lifetest this failure mechanism had been observed, resulting in

an increase in thruster recycle frequency and reduction in ion optics perveance. Therefore at 184.5 hours, the high voltage was turned off to the ion thruster to permit the installation of an oscilloscope to examine the output voltage of the accelerator, and screen supplies. No significant change (from that measured prior to the lifetest) in voltage ripple was identified on either supply. At that point, some preventative maintenance was conducted (including installation of new electrical contacts for the primary drive motors) on both supplies, and the thruster was brought back on-line to full power. During the 2 hour down period, the thruster discharge and neutralizer remained on.

Events #2, and #4-7 were all occurrences of the thruster discharge extinguishing during a high voltage recycle. Three of these events (#2, 4 and 5) resulted in the complete shutdown of the thruster, as commanded by the autonomous shutdown system triggered by a low discharge current sensor. Events #6 and 7 occurred while the authors were present and in both instances the discharge was immediately restarted and the thruster was brought back up to full power without being commanded off. Based on an examination of the strip-chart data during the test, all five discharge-out events occurred half-way through a recycle at the point where the high voltage was reapplied to the ion optics. When the high voltage was reapplied, a simultaneous high beam current pulse greater than 5.0 A was observed, along with an immediate drop of the discharge current from the recycle cut-back value to zero amperes (extinguishing the discharge). The high current pulse was interpreted as electron-backstreaming from the neutralizer cathode, exacerbated by the slow recovery speed of the motor driven high voltage supplies. Under any circumstances, however, a high current breakdown during a recycle could result in the plasma discharge being extinguished because the transistorized series pass current regulator on the discharge power supply was set to maintain a fixed discharge current. The discharge current is the sum of the cathode emission current (electrons from the discharge hollow cathode) and the beam current (electrons from the beam ions). During the high-voltage recycle sequence the cut-back value of the discharge current was originally set at 8.0 A, reduced from a run value of 22.0 A. If a transient pulse greater than 5.0 A was sensed on the beam current circuit (such as during electron-backstreaming) when the high-voltage was released, the cathode emission current would be reduced to zero or near-zero to maintain a fixed discharge current, resulting in the plasma discharge being extinguished. This hypothesis was tested by incrementally increasing the discharge current cut-back value until after event #7 the cut-back was set at 12.0 A, whereupon no further discharge-out events were experienced for the remaining 265 hours of the test. The 12.0 A current setting was high enough to sustain the discharge even during a high current breakdown mid-way through a high-

voltage recycle. Had a cathode emission current control logic been employed on the discharge supply regulator these events would not have occurred. The total elapsed thruster-off time for events #2 and 4-5 was 14.2 hours. The total beam-off time for events #6 and 7 was 0.2 hours.

Event #3 occurred at run hour 317.7 when the high voltage and neutralizer supplies were commanded off to permit repair of the neutralizer keeper supply. As will be discussed in a following section, the neutralizer experienced a performance degradation during the test; the keeper supply may have contributed to the degradation. Low frequency (approximately 1 Hz) oscillations of the neutralizer keeper voltage were observed on the chart recorder intermittently from the beginning of the lifetest. These were accompanied by intermittent low frequency oscillations in the keeper current beginning at about run-hour 185, immediately after test event #1. At run hour 317 the frequency of these oscillations increased, at which point the neutralizer keeper current was examined on an oscilloscope and found to be half-wave 120 Hz, 0-to-3.0 A peak output (as opposed to a 3.0 A dc level). At run hour 317.7 the ion beam and neutralizer were commanded off. Upon examination of the neutralizer keeper supply, the output filter capacitor appeared damaged and was replaced. The output current of the keeper supply was then found to be acceptable, with only a +/- 0.1 A ripple at 3.0 A output. The thruster was subsequently brought to full-power and the test was restarted. Total elapsed beam-off and neutralizer-off time was 4.5 hours, during which time the discharge remained on.

At run hour 890.0 the thruster was commanded off to permit installation of a new fully-charged xenon propellant bottle. Upon restarting the thruster the neutralizer keeper sustained damage, at which point it was decided to terminate the lifetest. Prior to removal of the thruster from vacuum, the thruster, minus-neutralizer, was restarted (with neutralizer common grounded to the facility) to obtain discharge chamber and ion optics (perveance) performance. During this period the thruster was operated at a variety of throttled conditions for approximately 1.4 hours.

Thruster Performance

Table IV summarizes the thruster operating and performance parameters at several different times during the lifetest (and post-test). Also presented are the average parameter values and their variations over the lifetest. The data were obtained from manually recorded parameters, and reduced in the manner described in Appendix B. As indicated, the average test conditions were 5.5kW input power at approximately 3800 seconds specific impulse and 68 percent overall thruster efficiency, providing a thrust of approximately 0.20 N.

Figures 7 and 8 respectively, show the overall thruster efficiency and specific impulse versus time for the 890.0 hour lifetest duration. As indicated in Figure 7, the thruster experienced an overall efficiency decay of approximately 5.6 percent, from 71-to-67%. A corresponding reduction in specific impulse is observed in Figure 8, going from approximately 4000 seconds down to 3800 seconds. The decrease in both the thruster efficiency and specific impulse follow a one-to-one correspondence with the decrease in total propellant efficiency over the test duration (Figure 9). The decrease in propellant efficiency was essentially due to two factors. First, a decay in neutralizer performance over the test duration necessitated gradually increasing the propellant flow rate through the neutralizer in an attempt to stabilize its operation. Second, the beam current decreased monotonically over approximately the first two hundred hours due to a decrease in the screen supply output voltage. Figure 10 shows overall thruster efficiency versus specific impulse obtained over the lifetest duration. The curve is broken into two bands; a high efficiency band of data during the run hours 0-to-291.5, and a lower efficiency band for the remaining 598.5 hours. The step-function decrease in efficiency is associated with an increase in the neutralizer power and mass flow rate at 291.5 hours (on restart after event #2). It is noted here that no irreversible thruster performance degradation was experienced over the lifetest other than that which is directly attributable to the neutralizer operation. This is discussed in more detail in the 'Post Test Thruster Analyses' section.

Figure 11 shows the fluctuations in the thruster input and beam power over the test duration, which are approximately +/- 5 percent in magnitude. Both power levels track closely, with the beam power constituting approximately 89 percent of the total input power to the thruster. The fluctuations in the power levels are due to changes in the output voltage set point of the screen supply, which occur after each high-voltage recycle. The screen supply output voltage variations impact the thruster power level in two ways: firstly, the variations change the beam voltage; secondly, the variations mean that the total accelerating voltage across the ion optics is changing, which results in variations in the beam current which show up as changes in power level as well. Figure 12 shows the time fluctuation of the thrust, approximately +/- 5 percent. Again, the variations are due to changes in the screen power supply output voltage, as the thrust is proportional to the beam current, and to the square root of the beam voltage.

The following sections describe the performance during the lifetest of each of the major thruster components.

discharge chamber and discharge cathode assemblies - The discharge losses (or beam ion production cost) over the lifetest duration are plotted in Figure 13. The losses, a measure of the electrical efficiency of the discharge, vary by

approximately +/- 5 percent over the test from an average value of 158 watts per beam ampere. These variations reflect changes in the beam current and the discharge voltage. The variations in discharge voltage (Figure 14) with time were due to drift in the propellant mass flow rate through the discharge cathode. The vertical striations in the discharge voltage data correspond to points during the lifetest where a manual re-adjustment of the cathode flow rate was made. Figures 15 and 16 show the variations in discharge cathode and main plenum propellant mass flow rates, respectively, over the lifetest duration. The variations were caused by small changes in the propellant delivery pressure downstream of the second gas regulator, due to the sensitivity of the regulator to cyclic changes in the ambient laboratory temperature. Note that the indicated-to-true correction factor for the metered propellant flow rates was greater than 1.6, with the precision of the mass flow meter read-out for the cathode and main lines being 0.1 and 1 sccm respectively. The combined variation in discharge losses and propellant efficiency is shown in Figure 17.

ion optics - Figures 18a and 18b show the high-voltage recycle rate, and cumulative number of recycles, for the lifetest duration. Noteworthy is that the recycle rate increased with test time for approximately the first 150 hours in a step-wise fashion, after which a fairly constant rate of 2.4 recycles/hour was observed for the remaining 740 hours. The first 25 hours of testing experienced a rate of 0.2 recycles/hour; the second 25 hours experienced a rate of 0.4 recycles/hour. From hour 50 to 150, the rate was approximately 0.8 recycles/hour, until at hour 151 when the rate jumped by a factor of three to 2.4 recycles/hour. The rate magnitude and rate increase of recycles with time are generally atypically of most extended-duration ground tests of ion thrusters. Typically the arc frequency decreases over the first several hours of a test, during a 'clean-up' period, and then maintains a fairly constant rate of 0.2-0.5 recycles/hour. The low initial recycle rate during this test is believed to be due to the precautions taken prior to the test to insure a 'clean-room' assembly of the thruster. The increase in recycle rate with time may be due to a high arrival rate of graphite from the beam target. This contaminant, in combination with high charge-exchange erosion of the accelerator grid, probably resulted in formation of whiskers. This mechanism however would not appear to explain the step-function increases in recycle rate experienced during the test. Based on pre- and post-test leakage resistance measurements of the thruster, no significant loss in insulation properties was identified which could have contributed to the high recycle rate. Visual observations of the thruster made during the lifetest recycle events were also inconclusive as to an agent. Of several dozen recycles visually observed during the

test, approximately half occurred simultaneously with multiple-arcing events on the downstream center surface of the accelerator grid, and the others occurred with no visible arcing.

The role of a facility contaminant in causing a high recycle rate was evident during pretest extended-duration experiments. Three of five pretests experienced recycle rates of 0.5-to-1.6 recycles/hour, under conditions of hydrocarbon contamination of the thruster due to improperly trapped oil diffusion pumps. Without alteration to thruster hardware, this rate was reduced to 0.02-0.06 recycles/hr on the last two tests by improved trapping. These tests were conducted in a facility with a thruster-to-molybdenum beam target distance of approximately three times greater than the thruster-to-graphite target distance in the lifetest facility.

The variation in output voltage of the two high voltage grid supplies are shown in Figures 19 and 20. The only manual change in the output voltage of either supply was an adjustment to the limit set-points of the accelerator grid supply at hour 384.3. At that time it was believed the high recycle rate could be due to an enlargement of accelerator grid apertures. This would reduce the maximum permissible R-ratio (lower the backstreaming limit) to near that value obtained when the accelerator supply output voltage was at the lower set-point. However as indicated in Figure 18, no significant reduction in recycle rate was observed with the increase in accelerator supply output voltage.

Figures 21 and 22 show the time variation of the beam and accelerator grid impingement currents respectively. The beam current variation (+/- 3 percent) follows the variation in the screen supply output voltage. The charge-exchange ion contribution to the accelerator grid impingement current should be proportional to the product of the beam current and the neutral atom density; the accelerator current appears to follow this parameter fairly well. The decrease in average accelerator current after restart on hour 291.5 may be associated with a reduction in direct ion impingement due to improved beamlet focussing due to the screen grid voltage increase. However, the average net-to-total accelerating voltage ratio (R-ratio) was lower after hour 384.3, implying degraded focussing, and a deeper potential well to trap charge-exchange ions, but no commensurate increase in the average impingement current was observed.

neutralizer assembly - The neutralizer performance decayed during the lifetest. For approximately the first 110 hours of the test, the neutralizer keeper voltage monotonically increased (from approximately 18 to 21 volts), after which the voltage stabilized somewhat (Figure 23). During this period the neutralizer mass flow rate was permitted to drift upwards to mitigate the keeper voltage rate of change (Figure

24). Also for the duration of the lifetest, the neutralizer common-to-facility ground voltage monotonically increased from approximately -13 to -17 volts (Figure 25). In addition to the voltage increase, at approximately run hour 1.8, low frequency (about 1 Hz) oscillations of the keeper voltage (up to +/- 0.4 V) were observed on the strip chart recorder and metering, and continued (at various amplitudes and frequencies) on an intermittent basis until the keeper power supply problem was identified and resolved at run hour 317.7. During the oscillations, the keeper voltage could be stabilized by small (approximately 10 mA) increases in the propellant flow rate through the neutralizer line, but the oscillations would eventually return.

After event #2, during which the thruster shut down, the neutralizer cathode would not restart under normal activation procedures, and did not start until the main discharge cathode was started. At this point (run hour 291.5) the neutralizer operating condition was modified by increasing the keeper current from 2.5 to 3.0 A, and the mass flow rate from approximately 4.3 to 5.0 sccm. This was done to stabilize the current and voltage oscillations (identified later as power supply related) and to reduce the keeper voltage transient during a high-voltage recycle (during which period the keeper voltage would climb to greater than 30 V due to the reduced emission current requirement and the length of the recycle period). After repair of the keeper supply at hour 317.7 and thruster restart, an attempt was made to return the neutralizer to the original operating point (mass flow rate and keeper power). This resulted in a rapid increase in both keeper and coupling voltages, so therefore the neutralizer was returned to the modified operating condition. This indicated that the neutralizer had suffered an irreversible degradation in performance. The neutralizer operating point was maintained at the modified condition for the remainder of the test. All subsequent restarts of the neutralizer cathode (after events #3-5) occurred only after ignition of the discharge cathode, an abnormal activation.

After shutdown, propellant bottle change-out, and thruster restart at 890.0 hours, the neutralizer cathode failed to restart even after discharge cathode ignition. During attempts to restart the neutralizer, a high-voltage discharge occurred from neutralizer keeper-to-common whereupon all neutralizer power was removed, and the lifetest terminated. Final performance characterization of the thruster discharge and ion optics was conducted with the neutralizer common grounded.

Ground Support Equipment Performance -
As discussed in the test chronology and thruster performance sections, variations in thruster performance, and operational problems such as thruster shut downs, were due in large measure to the performance of the laboratory power supplies. These include: (1) poor output voltage regulation and control of both the screen and accelerator grid supplies and the slow recycle sequence due to their motor drives (which potentially created conditions conducive to electron-backstreaming, and resulted in large voltage transients of the neutralizer keeper and discharge voltage as the recycle time was significantly longer the thermal time constant of the hollow cathodes); (2) failure of the neutralizer keeper supply output filter network, which may have contributed to the neutralizer assembly failure; and (3) use of a discharge current regulation mode (vs. cathode emission current), resulting in a condition which permitted high beam current transients to quench the discharge plasma. The propellant feed system also contributed to thruster performance variations. This was because the propellant delivery pressure to the metering valves varied due to a sensitivity of the gas regulator to changes in ambient temperature. This resulted in mass flow rate variations of +/- 50 mA on the main plenum line, and more importantly +/- 11 mA on the hollow cathode lines. Consequently some manual adjustment of the propellant flow rates was necessary during the lifetest.

One of two strip chart recorders failed during the lifetest and was replaced. This resulted in the loss of approximately 7 hours of thruster data, from run hour 128 to 135. The performance of the vacuum test facility was nominal over the lifetest duration. A facility pressure of 1.7×10^{-3} Pa was maintained for the test duration.

Post Test Thruster Analyses

After completion of the lifetest and prior to removal of the thruster from vacuum, tests were conducted to characterize the discharge chamber and ion optics performance. The results of these tests are presented in the following section, including a comparison of these data to that obtained prior to the start of the lifetest. Follow-on experiments were also conducted on the lifetest neutralizer hollow cathode to verify the failure mechanism, the results of which are presented. Finally, post-lifetest examination and documentation procedures are presented, along with preliminary results and interpretations of component erosion and other wearout mechanisms observed.

Performance

As previously mentioned, no irreversible thruster performance degradation (specific impulse, thrust, propellant and electrical efficiencies and overall thruster efficiency) was experienced over the lifetest within the measurement uncertainties, other than that which is directly attributable to the decay in the neutralizer performance. This was demonstrated in two fashions: first, immediately following the lifetest, thruster performance data were obtained without neutralizer operation and normalized assuming a fixed neutralizer operating condition; and second, after preliminary

9

hardware documentation of the thruster was completed, the thruster was reassembled and the performance was characterized with the lifetest neutralizer cathode operational. For both test conditions, the thruster performance was essentially identical to that obtained prior to the start of the lifetest. This was because the thruster did not experience any appreciable loss in discharge chamber or ion optics performance over the lifetest duration. The post-test performance of the major thruster components are presented in the following sections.

discharge chamber and discharge cathode assemblies- A comparison of pre- and post-lifetest discharge chamber performance curves are presented in Figure 26. The curves were obtained by varying the discharge current, at fixed main plenum and discharge cathode propellant flow rates. As indicated, no significant change in the discharge losses or discharge propellant efficiencies were experienced. This was the case despite a measurable increase in accelerator grid apertures during the lifetest.

Figure 27 presents the current-voltage characteristic data for the discharge before and after the lifetest. Although the discharge voltage after the lifetest is somewhat higher at throttled conditions the data begin to converge at high discharge currents.

ion optics - Perveance data taken before and after the lifetest (beam current versus total accelerating voltage) are presented in Figure 28. For a given beam current, the minimum total voltage decreased by an average of approximately 120 V. This increase in perveance is believed to be entirely associated with an increase in accelerator grid aperture diameters, due to ion machining, occurring predominantly at the outer beam edge, which were identified during post-test examination of the grids. No other change in ion optics geometry such as in the cold-gap or alignment was identified.

neutralizer assembly - Failure of the neutralizer assembly resulted in the termination of the lifetest. Consequently no performance mapping of the neutralizer was possible prior to the removal of the thruster from vacuum. Upon removal from vacuum it was discovered that a catastrophic failure of the neutralizer keeper mounting structure had been experienced at the 890.0 hour restart. At this point it was hypothesized that the neutralizer performance degradation experienced over the lifetest was associated with a mechanical failure of the keeper bar support (a gradually increasing misalignment of the keeper bar with respect to the hollow cathode) and was not associated with a degradation of the neutralizer cathode proper. Consequently an experiment was conducted to characterize the operability of the neutralizer cathode. This was done by retesting the thruster with the lifetest

neutralizer hollow cathode, with a new keeper assembly identical in geometry to that used for the lifetest. The operating characteristics of the neutralizer cathode, in terms of keeper voltage versus mass flow rate at various keeper currents, were comparable (within +/- 1 volt) to the initial conditions demonstrated at the start of the lifetest, data which strongly supports the hypothesis of keeper bar support failure.

Hardware

After the lifetest, a thorough examination of the thruster and test facility was performed, and at this writing a preliminary analysis of the results obtained from the thruster hardware has been completed. Details of the thruster examination and a cogent summary of the results of the analysis are presented in the following sections.

examination and documentation procedures - Every effort was made in the post-test examination and analysis of the lifetest thruster to preserve all possible observable characteristics. After removal from the vacuum chamber, the analysis began with a complete visual inspection and photo-documentation of the ion thruster on the test stand. Leakage resistance measurements of the thruster were made at this time, as well as physical measurements and collection of flakes and deposition samples exterior to the thruster proper. Photo-documentation, measurements, and sample collection continued as the thruster was disassembled on the test cart. Major components of the thruster were removed (ion optics, neutralizer and discharge cathode assemblies) at this time and were prepared for further close-up photography, measurement, and disassembly.

Prior to a complete disassembly of the discharge chamber, magnetic field mapping was conducted, and attempts were made to remove deposition samples from internal anode surfaces. Close-up photography was conducted on the ion optics to quantify aperture alignment, and grid-to-grid spacing measurements were made. The optics were then disassembled for thickness and mass measurements of the grids and measurements of aperture diameters, and further photography. The neutralizer and discharge cathode assemblies were photographed, and measurements were made of the orifice plate geometries. Preliminary scanning electron microscopy (SEM) micrographs were taken of both discharge and neutralizer cathodes, and of the discharge cathode assembly starting electrode. In addition, x-ray microanalysis (Energy Dispersive Analysis by X-rays, or EDAX) was performed to determine the elemental composition of sputtered material coatings on some thruster insulators.

results and interpretations - A preliminary examination of the thruster components while still on the test cart indicated that several had survived the

lifetest with little or no damage. These undamaged components included most thruster structural elements and insulators, and all wiring. Components which had been damaged extensively were the neutralizer keeper bar and the neutralizer keeper support rod and ceramic insulator. In addition, severe erosion was evident on the downstream surface of the accelerator grid (due to charge-exchange) and on the discharge cathode assembly starting electrode.

Results obtained from analyses of the major thruster components include:

discharge chamber -
- Within the measurement uncertainty there was no change (irreversible losses due to thermal degradation) in the discharge magnetic field.

- There was negligible deposition, and no spalling of material, on the internal anode surfaces (Figure 29).

discharge cathode assembly -
- The discharge cathode starting electrode underwent severe erosion due to ion sputtering. The electrode length was reduced by approximately 0.92-cm, as it was honed back to a fine point (Figure 30). Total electrode mass loss is estimated to be greater than 0.070-gm. (see Appendix C for further discussion)

- The minimum discharge cathode orifice diameter decreased from an initial value of 0.16-cm to a mean diameter of 0.12-cm, a decrease in area of 42 percent. The reduction in diameter is due to deposition of material onto the orifice plate at the throat of the chamfer. SEM analysis of the material indicates that its structure is consistent with surrounding orifice plate material. Elemental analysis, via EDAX, indicates that the deposited material consists of tungsten. An examination of the interior surfaces of the discharge cathode insert using a micro-borescope indicate that the tungsten insert may have undergone ion bombardment and appears to be un-sintered. Destructive dissection of the hollow cathode and further analyses will be required to determine the mechanism(s) which resulted in the tungsten deposition on the orifice plate chamfer, and the change in insert condition.

The surrounding orifice plate area is roughened, presumably from ion bombardment, to the degree that original machining grooves in the tungsten surface are no longer visible (Figure 31). Most exterior surfaces of the hollow cathode tube and heater assembly appeared to be in prisitine condition, except for a dulled area, possibly due to ion sputtering, on the tube immediately upstream of the heater coils. Within the measurement uncertainty of about 5.1 microns,

however, no change in cathode tube outside diameter could be identified at this location. The tantalum foil wrap on the heater coils appeared pristine.

- Cathode assembly high temperature ceramic insulators in the discharge were coated with molybdenum and rhenium, as identified by EDAX. The deposited material appears to have originated from sputtering of the discharge cathode tube in the region upstream of the heater coils (see Figure 30). Traces of aluminum and tantalum were also present on the ceramic sheath of the starting electrode.

ion optics -
- Within the measurement uncertainty there was no change in the assembled grid-to-grid cold-gap or alignment.

- The accelerator grid suffered a mass loss of 17.759 gm +/- 0.004 gm over the 956.8 hour test period, consisting of the 890.0 hour 5kW lifetest plus pre- and post-test operation (including 16.0 hours at 5kW, and 50.8 hours at a variety of throttled conditions).

Charge-exchange erosion pits penetrated the entire thickness of the molybdenum accelerator grid (0.36-mm) from the geometric center of the ion optics out to exactly half-radius (see Figure 32). The upstream surface holes of the charge-exchange pits are greater than 0.015-cm in diameter near the electrode center. There is no evidence of localized charge-exchange associated with the neutralizer. Appendix D contains a further discussion of the charge-exchange erosion.

The accelerator grid aperture diameters, out to half-radius, enlarged uniformly by an average of 0.038-mm.

Ion-machining, presumably due to beamlet over-focusing, is evident on the outer seven rows of holes (Figure 33). There is a deposition of aluminum on the extreme downstream outer radius of the grid, believed to be due to sputtering of the back surface of the front ground plate from highly divergent beam ions.

- The screen grid incurred a mass gain of 0.711 gm +/- 0.004 gm over the test period, due to deposition of molybdenum from the accelerator grid erosion (see Figures 34 and 35).

Within the measurement uncertainty there was no change in screen grid thickness over the entire grid diameter. Based on the measurement uncertainty a maximum grid thickness decrease of 5.1 microns is possible.

There was no visual evidence of erosion at any location on the screen grid (see Figures 34 and 35) and there was no discernable change in screen grid aperture diameters.

neutralizer assembly -
- There is evidence of direct ion interception of the neutralizer hollow cathode via energetic high angle beam ions (Figure 36); tantalum foil on the beam-facing surface of the heater sheath was sputter-eroded (see Appendix E for further discussion).

- The minimum neutralizer cathode orifice diameter increased from an initial value of 0.051-cm to a diameter (mean) of 0.064-cm, an increase in area of 56 percent (Figure 37). Under SEM and EDAX analyses some deposition of tungsten was evident around the orifice plate chamfer.

- The neutralizer keeper bar was severed from the keeper rod, and the rod and ceramic were melted into a eutectic. This damage occurred during restart at hour 890.0, and is believed to be due to a high-voltage, low-current discharge from neutralizer common-to-neutralizer keeper support rod. At that point the closest cathode-to-keeper potential gap was from orifice plate to the keeper rod tip. The current attachment did not occur on the keeper bar, as this component had translated under gravity away from the cathode orifice plate due to the failure of the single point mechanical attachment under repeated thermal cycles.

These results are summarized in Table V. Based on leakage resistance measurements made before and after the lifetest, no significant deterioration in insulation was identified.

The following conclusions can be drawn from an interpretation and analysis of the results obtained from the post-test examination of the thruster components:

- The magnet materials experienced no irreversible losses in properties, indicating the material selection and thruster thermal design are adequate for 5kW power-level extended-duration mission applications.

- Although no performance decay of the discharge and neutralizer hollow cathodes was experienced during the lifetest, the anomalous material formation on the orifice plates necessitates a complete physicochemical analysis of the lifetest cathode materials. The apparent change in discharge cathode insert condition, and the sputtering of the discharge cathode tube also require further investigation.

- The starting electrode erosion is unacceptably high and will necessitate a concept/design modification to the thruster.

- Charge-exchange ion erosion of the accelerator grid is a primary factor in life limitation. Under the present ground test conditions and 5kW operating point, the accelerator grid would be expected to suffer a catastrophic structural failure as early as 4200 hours. However, in space-like environmental conditions, the accelerator grid lifetime is expected to be in excess of 11,500 hours (see Appendix D). It is imperative that the charge-exchange processes responsible for the high grid erosion be more thoroughly understood, and that the accelerator grid erosion be quantified with high certainty under space-like environmental conditions. To do so will require low-pressure testing at 5kW in helium-cryopump equipped facilities.

- Screen grid erosion by discharge ions is not a factor in thruster wearout lifetime. The 5.1 micron thickness measurement uncertainty implies a maximum possible erosion rate of approximately 6 microns per 1000 hours. The screen grid has a beginning-of-life thickness of 360 microns, which should permit at least 35,000 hours of operation before it wears to half thickness. Based on an analysis of the residual facility gases, it was found that the no-load base pressure of 6.7×10^{-5} Pa was due to approximately 50 percent water vapor and 50 percent nitrogen. Reference 10 has shown that the presence of reactive residual gases (including nitrogen and water vapor) can reduce the sputter yield of molybdenum by forming a surface compound that has a lower sputter yield than the base metal. However, the magnitude of this effect with water vapor has not been quantified. Therefore, it was assumed that the water vapor was as reactive as nitrogen. From data of reference 10 and facility effect curves in reference 11, the impact of the reactive residual gases on screen grid erosion during the lifetest is believed to be negligible. This may provide some leverage in addressing the accelerator grid erosion, vis-a-vis operation at higher propellant efficiencies. However this will necessitate improved propellant flow regulation.

- The neutralizer assembly will require a redesign and performance optimization. The erosion rate of the cathode assembly due to direct ion interception is sufficiently low that an addition of low sputter coefficient material should prevent penetration of the housing. However, a study should be initiated to optimize the position of the neutralizer with respect to the ion beam.

12

Thruster Modifications

Two second-generation laboratory model ion thrusters are being fabricated at NASA-LeRC which incorporate design modifications to eliminate or minimize problems identified by the 5kW lifetest. These thrusters, identical in essentially all respects, are based on common design criteria established by both NASA-LeRC and Hughes Research Laboratories. After an initial performance characterization of both thrusters at NASA-LeRC, one will be transferred for testing at Hughes. This 5kW 'common' thruster approach will insure the capability of establishing common protocols and procedures and will maximize repeatability and transportability of results.

One of the most significant problems identified by the lifetest was the starting electrode erosion. The erosion level was so high as to warrant elimination of this component from the common thruster design. The starting electrode was incorporated in the lifetest thruster to facilitate discharge cathode ignition, as the thruster design did not incorporate a keeper geometry. However prior to and during the conduct of the lifetest, thruster discharge ignition was achieved on several occasions without the use of the starting electrode (without a high-voltage breakdown). Discharge ignition would occur immediately upon turning on the 80 V open circuit discharge supply voltage to the anode, under normal propellant flow conditions, after a period of cathode pre-heating. Subsequent to the lifetest, experiments at both NASA-LeRC and Hughes have demonstrated reliable discharge ignition directly off of the anode, without the requirement of a starting electrode or keeper.

The poor performance, and performance degradation, of the neutralizer assembly was also a significant problem during the lifetest. The second-generation laboratory model thruster incorporates a neutralizer assembly with a mechanically-robust enclosed keeper structure, similar in geometry to that developed by Hughes for the XIPS thruster[4]. The XIPS neutralizer has demonstrated superior performance in terms of propellant mass flow rate and power requirement to the lifetest assembly, albeit at a lower cathode emission current requirement. Steps are also being taken to address the ion beam interception of the neutralizer including the ability to vary in-situ the neutralizer position with respect to the ion beam.

Ground Support Equipment Modifications

As previously discussed, to a considerable degree the performance of the thruster was impacted by non-thruster operational problems attributable to power supplies and propellant regulation. Subsequent to the lifetest and prior to the initiation of further extended-duration tests, a number of upgrades are being incorporated. These include the installation of a new power supply system which includes: solid-state high voltage supplies capable of about 100 milli-second time scale recycle rates with precise output voltage control; capability to regulate cathode emission current, as opposed to discharge (anode) current; and integral digital oscillopes to continuously monitor power supply and thruster currents and voltages. Upgrades to the propellant feed system include installation of a flight-qualified precision gas pressure regulator for improved propellant regulation, and reduction in propellant feed line lengths and exclusive use of welded metal gasket face seal fittings (to reduce outgassing and leak rates). The modifications made to the thruster and ground support equipment to resolve problems identified by the lifetest are listed in Table VI.

Conclusions

This paper described the results obtained from the first lifetest of a high power ring-cusp ion thruster. A 30-cm diameter laboratory model ion thruster was operated steady-state at a nominal beam power of 5kW on xenon propellant for approximately 900 hours. This test was conducted to identify life-limiting erosion mechanisms and thruster design modifications, and to demonstrate operation using simplified power processing. It represents an initial effort to establish a 10,000 hour capability of a 5kW ion thruster, lifetime and power-level performance targets which are consistent with projected near-term Earth-space mission requirements.

The lifetest was essentially uneventful, with only minor problems associated with non-thruster ground support equipment. At run hour 890.0 the thruster was commanded off to permit installation of a new fully-charged xenon propellant bottle. Upon restarting the thruster the neutralizer sustained damage, due to failure of the structure supporting the neutralizer keeper electrode, and it was decided to terminate the test. The average performance parameters for the thruster over the lifetest duration were 5.5kW input power at approximately 3800 seconds specific impulse and 68 percent overall thruster efficiency, providing a thrust of approximately 0.20 Newtons.

An overall thruster efficiency decay of approximately 5.6 percent was experienced, over the lifetest, associated with a degradation in neutralizer performance. No other irreversible thruster performance degradation was experienced over the lifetest. The cause of the neutralizer performance loss and eventual failure was identified subsequent to the lifetest as due to a gradual shift in the neutralizer keeper mounting structure. It was the sudden complete failure of the structure which ended the lifetest. A new neutralizer design has been completed and implemented which promises to resolve the problems identified during the lifetest.

After the lifetest, a thorough examination of the thruster hardware was conducted. Most thruster components had

13

survived the lifetest with little or no damage. However, severe erosion was evident on the downstream surface of the accelerator grid due to charge-exchange ion impingement, and on the discharge cathode starting electrode. Based on an interpretation and analysis of the thruster components, the following conclusions can be drawn:

- Although no performance decay of the discharge and neutralizer hollow cathodes was experienced during the lifetest, the anomalous material formation on the orifice plates, and the apparent change in discharge cathode insert condition necessitates a complete physicochemical analysis of the lifetest cathode materials.

- The starting electrode erosion was so high as to warrant elimination of this component from the thruster design. Subsequent to the lifetest, experiments have demonstrated reliable thruster ignition using a new starting technique which eliminates the need for this component.

- Charge-exchange erosion of the accelerator grid is a primary factor in life limitation. To a significant degree, however, the high erosion is a facility effect associated with a high neutral background density of xenon atoms. In space the accelerator grid lifetime is expected to be in excess of 11,500 hours. It is imperative that the charge-exchange processes responsible for the high grid erosion be quantified with high certainty under space-like environmental conditions. To do so will require low-pressure testing at 5kW in helium-cryopump equipped facilities.

- The erosion of the screen grid by discharge ions is not a factor in thruster wear-out lifetime.

Acknowledgements

References

1. Sovey, J.S., "Improved Ion Containment Using a Ring-Cusp Ion Thruster," Journal of Spacecraft and Rockets, Vol. 21, No. 5, Sept.-Oct. 1983, pp. 488-495.

2. Rawlin, V.K., "Operation of the J-Series Thruster Using Inert Gas," AIAA Paper 82-1929, Nov. 1982.

3. Sovey, J.S., "Characteristics of a 30-cm Diameter Argon Ion Source," AIAA Paper 76-1017, Nov. 1976.

4. Beattie, J.R., Matossian, J.N., and Robson, R.R., "Status of Xenon Ion Propulsion Technology," AIAA Paper 87-1003, May 1987.

5. Rawlin, V.K., "Internal Erosion Rates of a 10-kW Xenon Ion Thruster," AIAA Paper 88-2912, July 1988.

6. Beattie, J.R., Hughes Research Laboratories, Private Communication.

7. Deininger, W.D., and Vondra, R.J., "Electric Propulsion for Constellation Deployment and Spacecraft Maneuvering," AIAA Paper 88-2833, July 1988.

8. Sponable, J.M., and Penn, J.P., "An Electric Orbital Transfer Vehicle for Delivery of NAVSTAR Satellites," AIAA Paper 87-0985, May 1987.

9. Patterson, M.J., and Curran, F.M., "Electric Propulsion Options for 10kW Class Earth Space Missions," Presented at 1989 JANNAF Propulsion Meeting, May 1989 (NASA TM-102337).

10. Beattie, J.R., "A Model for Predicting the Wearout Lifetime of the LeRC/Hughes 30 cm Mercury Ion Thruster, AIAA Paper 79-2079, Oct. 1979.

11. Rawlin V.K., and Mantenieks, M.A., "Effect of Facility Background Gases on Internal Erosion of the 30 cm Hg Ion Thruster," AIAA Paper 78-665, Apr. 1978 (NASA TM-73803).

12. Friedly, V.J., and Wilbur, P.J., "Hollow Cathode Operation at High Discharge Currents," NASA CR-185238, Apr. 1990.

13. Maloy, J.E., Poeschel, R.L., and Dulgeroff, C.R., "Characteristics of 30-centimeter Mercury Ion Thrusters," NASA TM-81706, Apr. 1981.

14. Massey, H.S.W, Burhop, E.H.S., and Gilbody, H.B., "Electronic and Ionic Impact Phenomena,"Recombination and Fast Collisions of Heavy Particles, Volume IV, Clarendon Press, Oxford, 1974, p. 2772.

15. Smirnov, B.M., and M.I. Chibisov, "Resonance Charge Transfer in Inert Gases," Soviet Phys. Tech. Phys., V. 10, No. 1, July 1965, pp. 88-92.

Appendix A: cathode activation procedure

Prior to the initiation of the lifetest, a preliminary hollow cathode activation procedure was developed for xenon propellant. These efforts were motivated by failures experienced with laboratory ion thruster cathodes during a prior lifetest[5]. The cause of these and other failures were later identified as oxidation, resulting in tantalum tube embrittlement and poisoning of the low work function insert. The oxygen is suspected to be present in the cathode insert as water, both adsorbed water molecules during exposure to the ambient laboratory environment, and water molecules bound to the impregnant. Other sources of possible oxygen contamination include outgassing and leaks in the propellant feed system, and impurities in the propellant gas.

To address these issues a preliminary procedure for cathode activation was developed and implemented during the course of the lifetest program. The procedure involves: (1) minimizing exposure of the cathode inserts to ambient laboratory conditions; (2) maintaining a constant argon purge through the hollow cathodes, while the cathodes are mounted in the thruster, during all non-testing periods (both in atmosphere and at vacuum); (3) initiating and maintaining a xenon propellant purge through the hollow cathodes prior to and during pre-heating of the cathode inserts; and (4) pre-heating the cathodes using incremental heater power to increase the cathode tube temperature from ambient-to-1100 degrees centigrade in one hour. In addition the exclusive use of molybdenum or molybdenum-rhenium for cathode body tubes has been selected, as these materials do not embrittle under oxidation. Evaluation of the success of this procedure awaits a physicochemical analysis of the lifetest cathodes to identify whether any thermochemical reactions occurred.

Appendix B: thruster performance calculations

The thruster performance presented in the paper were generated primarily from a reduction of data from directly-measured parameters. All quoted propellant efficiencies include an estimated correction to the mass flow rate for propellant ingested from the facility.
For completeness, all first-order thruster performance parameters (thrust, specific impulse, and overall thruster efficiency) presented in the paper include a thrust loss which is the product of a beam divergence factor (estimated at 0.98) and a doubly-charged ion factor (estimated from ion beam charge state documentation of xenon ion thrusters). However, for ease in direct comparison to previously published data, the propellant efficiencies presented in the figures are uncorrected for doubly-charged ions. As previously indicated, all power supplies/metering and propellant mass flow rates were calibrated prior to the lifetest.

Appendix C: discharge cathode starting-electrode erosion

As indicated in the text, the stainless steel starting electrode suffered severe erosion over the period of the lifetest. Examination of the post-test geometry of the electrode macroscopically (Figures 38 and 39), and using SEM analysis, indicates that the erosion is due to ion sputtering. The high erosion rate indicates the presence of both a high ion current density, and high mean ion energy (greater than the cathode-to-anode potential difference). It is believed that the erosion of the electrode is such as to thin the diameter over its length. This would explain why no decrease in starting electrode length was observed during the preliminary extended-duration tests. In addition, the geometry of the ion-cleaned and sputter-deposited surfaces on the electrode insulator sheath, and the apparent preferential erosion of the electrode on the cathode-facing side, are highly suggestive of a spherical expansion of energetic ions from the region of the cathode orifice. This phenomenon (energetic ion production by a hollow cathode operating at high emission currents) may be the same as the 'jet ion' production observed and modelled by Friedly and Wilbur[12]. Their data suggest an inverse-square variation in the ion current density with axial position from the hollow cathode; this could in part explain why there was no discernable erosion of the upstream center of the screen grid over the period of the lifetest.

Appendix D: accelerator grid charge-exchange erosion

The erosion of the accelerator grid by charge-exchange ions appears to be the most serious and fundamental limitation which impacts the life expectancy of the 5kW xenon ion thruster. The end-of-life of the accelerator grid is considered to occur at the point when an equipotential surface can no longer be maintained. This should be commensurate with structural failure of the electrode due to ion erosion. Based on thickness measurements of the accelerator grid around the center apertures on the downstream surface (the location of maximum charge-exchange erosion), the minimum erosion depth surrounding the holes was found to be approximately 76 microns. Assuming a linear erosion rate with time (over the 906 hour period at 5kW), the grid material surrounding the center apertures would be severed from the electrode in approximately 4200 hours. This would result in accelerator grid material cantilevering into the screen grid to bridge the grid-gap, creating a short.
It is believed, however, that the apparent high charge-exchange ion production (and hence, high erosion rate of the accelerator grid) is to a significant degree a facility-enhanced effect. The evidence for this hypothesis includes the following:
(1) The accelerator grid impingement current has been shown to be a first order function of facility pressure (i.e.

background xenon neutral density; see Figure 40). Data of Figure 40 were taken with a 30cm xenon ion thruster at a fixed operating condition (power, propellant efficiency, and propellant mass flow rate) while the facility pressure was increased by bleeding xenon into the vacuum chamber at a location approximately 23 meters from the thruster. Extrapolating the data downward in pressure is believed to provide an approximate value of the accelerator grid impingement current due to the thruster (direct ion interception and charge-exchange from thruster neutrals), effectively subtracting the facility contribution. Although comparable data were not obtained for the lifetest thruster, a similar behavior would be expected. At the average lifetest condition of 17.5 mA accelerator grid impingement current and 1.7×10^{-3} Pa facility pressure, and assuming the same slope as the curve in Figure 40, a 'space-equivalent' accelerator grid impingement current of approximately 6.2 mA is estimated (or equivalently, a 0.19% ratio of accelerator impingement current-to-beam current, comparable to that obtained with mercury). This compares favorably to data obtained at Hughes using a similar methodology, indicating an accelerator grid impingement current of 5.8 mA at the 5kW condition[6].

(2) The accelerator grid impingement currents measured during operation of xenon ion thrusters are considerably higher than those previously reported for ion thrusters operating on mercury propellant. For mercury ion thrusters, with equivalent ion grid geometry as those reported for this lifetest, the ratio of accelerator grid impingement current-to-beam current was on the order of 0.15-0.17% for discharge chamber propellant efficiencies in the range of 95-89%[13]. At these ion velocities (aprroximately 2.5×10^6 cm/sec) the resonant charge-exchange cross-section for mercury is on the order of 5.3×10^{-15} cm^2 [14]. For the xenon lifetest thruster this ratio was approximately 0.55% at 93% discharge chamber propellant efficiency (see Figure 41), approximately 3.4 times higher than reported for mercury. At these ion velocities (3.8×10^6 cm/sec) the resonant charge-exchange for xenon is in the range of 4.5-to-7.0×10^{-15} [15]. Since the propellant efficiencies, cross-sections, and ion optics geometries are comparable, one would expect that the ratio of accelerator grid current-to-beam current would also be comparable, implying an equivalent charge-exchange ion production rate. The only apparent difference between these data which could impact the charge-exchange ion production rate are the reported facility pressures (i.e. propellant neutral density in the region of the ion optics due to facility pumping speeds), which for the xenon data are typically one-to-two orders of magnitude higher than the mercury data.

Assuming in space all the impingement current is due to charge-exchange ions collected on the downstream surface of the accelerator grid, and assuming an average accelerator grid impingement current of 6.2 mA at the 5kW operating condition, a reduction in accelerator grid erosion of approximately 2.8 would be anticipated from that observed in this lifetest. This would indicate an accelerator grid lifetime in space of greater than 11,500 hours.

Of a total accelerator grid mass loss of 17.759 gm, approximately 0.6 gm mass loss is estimated as due to ion machining of aperture holes from direct ion impingement, with the remaining 17.2 gm due to charge-exchange erosion on the downstream surface of the grid. The estimated mass loss due to charge-exchange erosion would require that a minimum of 10 mA of the accelerator grid impingement current be charge-exchange ions, with all ions arriving at normal incidence at an energy of 330 volts.

Appendix E: ion interception of neutralizer assembly

As evidenced by Figure 36, direct ion interception of the neutralizer occurred, resulting in sputter-erosion of the tantalum foil on the beam-facing surface of the heater sheath. The erosion was most severe at the tip of the cathode and reduced in magnitude moving upstream, indicating a gradient in the arriving ion current density. The total number of tantalum foil layers eroded at the cathode tip was approximately 10, while at the rear of the tube the number of eroded layers was 2. These levels correspond to etch rates from approximately 7.8×10^{-12} to 3.9×10^{-11} m/s. Using a gridded Faraday probe, ion current density measurements were made in the vicinity of the neutralizer cathode after the lifetest. At the nominal 5kW condition, a high energy ion current density of approximately 8.2 microamperes was measured, which would result in a tantalum etch rate of 1.5×10^{-11} m/s, which corresponds favorably to the measured erosion.

TABLE I.   —   Thruster/Lifetest Performance Targets.

Input power	>= 10kW steady-state [> 5kW for lifetest]
Lifetime	>= 10,000 hours at 5kW [lifetest duration >= 500 hours]
Effective specific impulse	3800 - 4000 seconds
Thrust	0.18 - 0.20 Newtons
Overall thruster efficiency	67 - 78%
Discharge/total propellant efficiencies	>= 90%/>= 85%
Discharge losses	<= 160 W/A
Discharge voltage	<= 28 volts
Beam current	> 3.0 amperes
Accelerator grid voltage	< 400 volts

TABLE II. — Thruster Design Parameters.

Discharge chamber
  exterior shell
    - material   0.15cm-thick 3-piece cold rolled steel

    - dimensions   34.6cm outside dia. by 24.6cm length

    - magnets   3 rings of Sm_2Co_{17}

  anode
    - material   0.23cm-thick grit-blasted aluminum alloy 6061

  main plenum
    - material   0.64-cm diameter stainless steel tubing

    - dimensions   mean ring diameter of 24.5cm

Discharge cathode assembly
  hollow cathode
    - material   Mo-41-Re tube with 2% Th-W orifice plate; porous
                          tungsten impregnated insert
    - dimensions   10.2cm-long by 0.64cm-outside diameter tube;
                          0.13cm-thick by 0.58cm-wide orifice plate;
                          0.15cm-diameter orifice

Ion optics
  grids
    - material   2-grid, SHAG geometry of 0.36mm-thick Mo (each grid)
    - dimensions   30cm-diameter (effective beam dia. of 28.2cm);
                          screen and accelerator grid apertures of 0.19cm and
                          0.11cm respectively

Neutralizer assembly
  hollow cathode
    - material   Mo-41-Re with 2% Th-W orifice plate; porous
                          tungsten impregnated insert; Mo keeper
    - dimensions   6.4cm-long by 0.64cm-outside diameter tube;
                          0.13cm-thick by 0.58cm-wide orifice plate;
                          0.05cm-diameter orifice

Total thruster mass   12.5 kg, excluding ground screen and wiring
                          harness

Power handling capability > 10 kW input power

18

TABLE III. - Summary of Pre-Lifetest Extended-Duration Tests.

Test #	1	2	3	4	5
Input power/beam power	5.7kW/4.9kW	5.7kW/4.7kW	5.7kW/4.9kW	5.7kW/4.9kW	5.4kW/4.7kW
Thrust	0.20 N	0.20 N	0.21 N	0.21 N	0.20 N
Overall thruster efficiency	70.3%	69.3%	70.0%	70.6%	70.5%
Specific impulse	3650 sec	3860 sec	3970 sec	3950 sec	3890 sec
Beam current	3.49 A	3.40 A	3.47 A	3.51 A	3.35 A
Discharge losses	188 W/A	195 W/A	189 W/A	172 W/A	164 W/A
Test duration	50 hours	73 hours	45 hours	50 hours	50 hours
# of high-voltage recycles	82	24	45	1	2
# of shutdowns	0	0	1 - commanded off	0	1- commanded off

TABLE IV. — *Lifetest Thruster Operating and Performance Parameters.*

											LIFETEST - AVERAGE	POST - TEST
run time, hours	0.0	101.6	195.8	295.5	405.1	505.4	600.1	699.3	800.4	890.0		
discharge voltage, volts	27.3	26.8	25.8	26.3	26.8	29.2	26.9	27.0	26.3	27.0	26.9	27.9
screen grid voltage, volts	1518	1497	1502	1569	1542	1536	1529	1520	1512	1514	1517	1425
accelerator grid voltage, volts	-321	-298	-304	-303	-373	-340	-338	-336	-337	-331	-331	-314
total accelerating voltage, volts	1853	1808	1817	1883	1927	1889	1878	1867	1859	1855	1860	1752
neutralizer keeper voltage, volts	18.5	20.8	20.1	20.2	15.8	16.2	16.1	16.7	17.0	17.2	17.8	15.5
neutralizer common-to-ground voltage, volts	-13.5	-13.9	-15.0	-15.0	-15.2	-16.2	-16.0	-16.0	-16.3	-17.0	-15.4	-15.0
discharge (anode) current, amperes	22.0	21.9	21.9	21.9	22.0	22.0	22.0	22.0	22.0	22.0	22.0	21.0
beam current, amperes	3.27	3.21	3.14	3.14	3.20	3.26	3.16	3.17	3.13	3.15	3.19	3.20
neutralizer keeper current, amperes	2.5	2.5	2.5	3.0	3.0	3.0	3.0	3.0	3.1	3.0	2.8	2.5
accelerator grid impingement current, milliamperes	18.0	18.0	18.0	17.8	16.9	16.0	16.9	17.2	17.9	16.5	17.4	24.0
corrected facility pressure, Pascals	1.7×10^{-3}	1.7×10^{-3}	1.7×10^{-3}	1.7×10^{-3}	1.7×10^{-3}	1.7×10^{-3}	1.7×10^{-3}	1.7×10^{-3}	1.7×10^{-3}	1.7×10^{-3}	1.7×10^{-3}	1.7×10^{-3}
propellant mass flowrates, amperes -												
– main plenum	3.12	3.10	3.11	3.01	3.11	3.01	3.08	3.05	3.12	3.04	3.09	3.06
– discharge cathode	0.27	0.27	0.29	0.29	0.30	0.30	0.29	0.29	0.31	0.31	0.29	0.28
– neutralizer cathode	0.22	0.23	0.27	0.33	0.34	0.34	0.35	0.35	0.37	0.35	0.32	0.28
– ingested flow	0.05	0.05	0.05	0.05	0.05	0.05	0.05	0.05	0.05	0.05	0.05	0.05
beam voltage, volts	1532	1510	1513	1580	1554	1549	1540	1530	1522	1524	1529	1438
R-ratio	0.83	0.84	0.83	0.84	0.81	0.82	0.82	0.82	0.82	0.82	0.82	0.82
discharge losses, W/A	156	156	154	157	157	168	160	160	159	162	158	155
total propellant efficiency, corrected for est'd J++, and for ingestion	0.87	0.86	0.83	0.83	0.82	0.85	0.82	0.82	0.82	0.80	0.82	0.85
total propellant efficiency, corrected for ingestion only	0.90	0.88	0.85	0.85	0.84	0.88	0.84	0.85	0.81	0.84	0.85	0.87
discharge chamber propel. eff., corrected for est'd J++, and for ingestion	0.92	0.91	0.89	0.91	0.90	0.94	0.90	0.91	0.88	0.90	0.90	0.92
discharge chamber propel. eff., corrected for ingestion only	0.95	0.94	0.91	0.94	0.93	0.97	0.92	0.94	0.90	0.93	0.93	0.94
beam ratio of J++/J+ [est'd]												
ion mass flow correction factor	0.07	0.06	0.05	0.06	0.06	0.08	0.06	0.06	0.05	0.06	0.06	0.07
beam divergence thrust correction factor	0.97	0.97	0.98	0.97	0.97	0.96	0.97	0.97	0.97	0.98	0.97	0.97
	0.98	0.98	0.98	0.98	0.98	0.98	0.98	0.98	0.98	0.98	0.98	0.98
J++ thrust correction factor	0.98	0.98	0.99	0.98	0.98	0.98	0.99	0.98	0.99	0.98	0.98	0.98
total thrust correction factor	0.96	0.96	0.97	0.96	0.97	0.96	0.97	0.96	0.97	0.97	0.96	0.96
thruster input power, watts	5640	5480	5360	5600	5600	5730	5500	5500	5400	5450	5510	5230
thruster beam power, watts	5010	4850	4750	4960	4970	5050	4870	4850	4760	4800	4880	4600
thrust, Newtons	0.20	0.20	0.20	0.20	0.20	0.20	0.20	0.20	195	0.20	0.20	0.19
thrust-to-power ratio, mN/kW	36.0	36.2	36.3	35.4	35.8	35.4	35.9	35.9	36.1	36.0	36.0	36.9
specific impulse, seconds	4010	3940	3820	3910	3840	3930	3800	3820	3700	3785	3840	3800
overall thruster efficiency	0.71	0.70	0.68	0.68	0.68	0.68	0.67	0.67	0.66	0.67	0.68	0.69

TABLE V. - *Summary of Lifetest Hardware Results.*

Discharge chamber
- no change in magnetic properties
- negligible deposition

Discharge cathode assembly
- severe erosion of starting electrode
- decrease in cathode orifice diameter
- change in insert physical condition
- cathode tube sputtering upstream of heater

Ion optics
- no change in grid-to-grid cold gap or alignment
- severe charge-exchange erosion of accelerator grid
- enlargement of accelerator grid apertures
- no change in screen grid thickness or apertures

Neutralizer assembly
- direct ion interception of cathode
- increase in cathode orifice diameter
- failure of keeper mechanical support

**TABLE VI. – *Modifications Incorporated to Solve Problems
Identified by Lifetest.***

VI. A – Thruster.

PROBLEM	MODIFICATION
Discharge Cathode and Starting Electrode	
(1) significant reduction in discharge cathode orifice diameter; change in physical condition of insert (2) excessive starting electrode erosion	(1) to be determined; improve integrity of propellant feed system (2) eliminate starting electrode; new starting technique demonstrated
Neutralizer Cathode Assembly	
(1) poor performance/performance degradation (2) direct interception of neutralizer cathode by energetic beam ions	(1) change to enclosed keeper geometry (2) reposition neutralizer and/or add low sputter yield coefficient graphite
Accelerator Grid	
(1) excessive charge-exchange erosion	(1) facility-enhanced effect; must be quantified to define 'in-space' lifetime; short-term testing with He cryopumping essential

VI B. – Ground Support Equipment.

PROBLEM (operational)	MODIFICATION
Power Supplies	
(1) poor voltage regulation; power supply failures	(1) new power supply system implemented, with solid-state high voltage supplies
(2) discharge-out during high voltage recycles	(2) control parameter changed from anode current to cathode-emission current
Propellant Feed System	
poor propellant mass flow rate regulation	integration of flight-qualified precision gas regulator into propellant feed system

Cross-section diagram labels (left):
- Anode Mounting Ring
- Samarium–Cobalt Magnet Rings
- Main Gas Plenum
- Starting Electrode
- Hollow Cathode
- Heater
- Ceramic Cathode Support
- Aluminum Anode Chamber
- Mild Steel
- Neutralizer

Dimensions: 24.5 cm (width), 34.6 cm (height)

Photograph labels (right):
- IRON SHELL
- ANODE
- CATHODE
- NEUTRALIZER
- DOWNSTREAM MAGNET RETAINER
- INSULATOR
- ION OPTICS

23

(A)   Cross-Section.
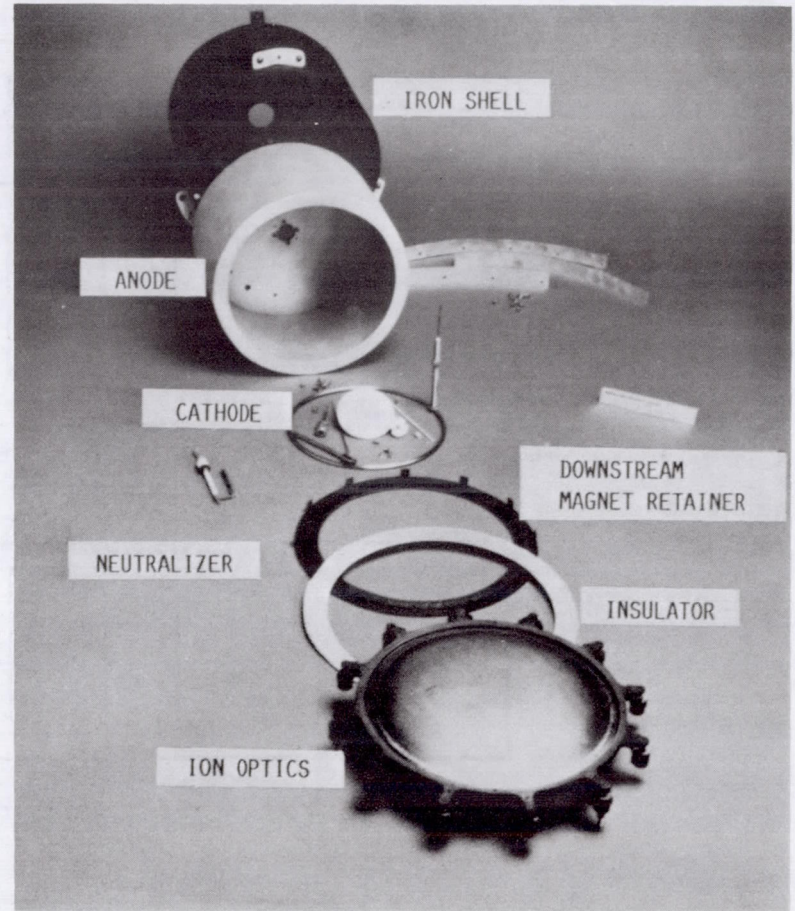
FIGURE 1.   -   30cm 5kW Laboratory-Model Lifetest
Xenon Ion Thruster.

THRUSTER

Accelerator grid

Discharge hollow
cathode

Anode

Screen
grid

Neutralizer hollow
cathode

ignitor
supply*
3kV

discharge
supply
27V/22A

Va

heater
supply*
14V/8A

keeper
supply
18V/2.5A

heater
supply*
14V/8A

Vd

Jd

Ja

+

+

−

Vs

Screen
supply
1.5kV/3.2A

Accelerator
supply
−330V/18mA

Jb

Vg
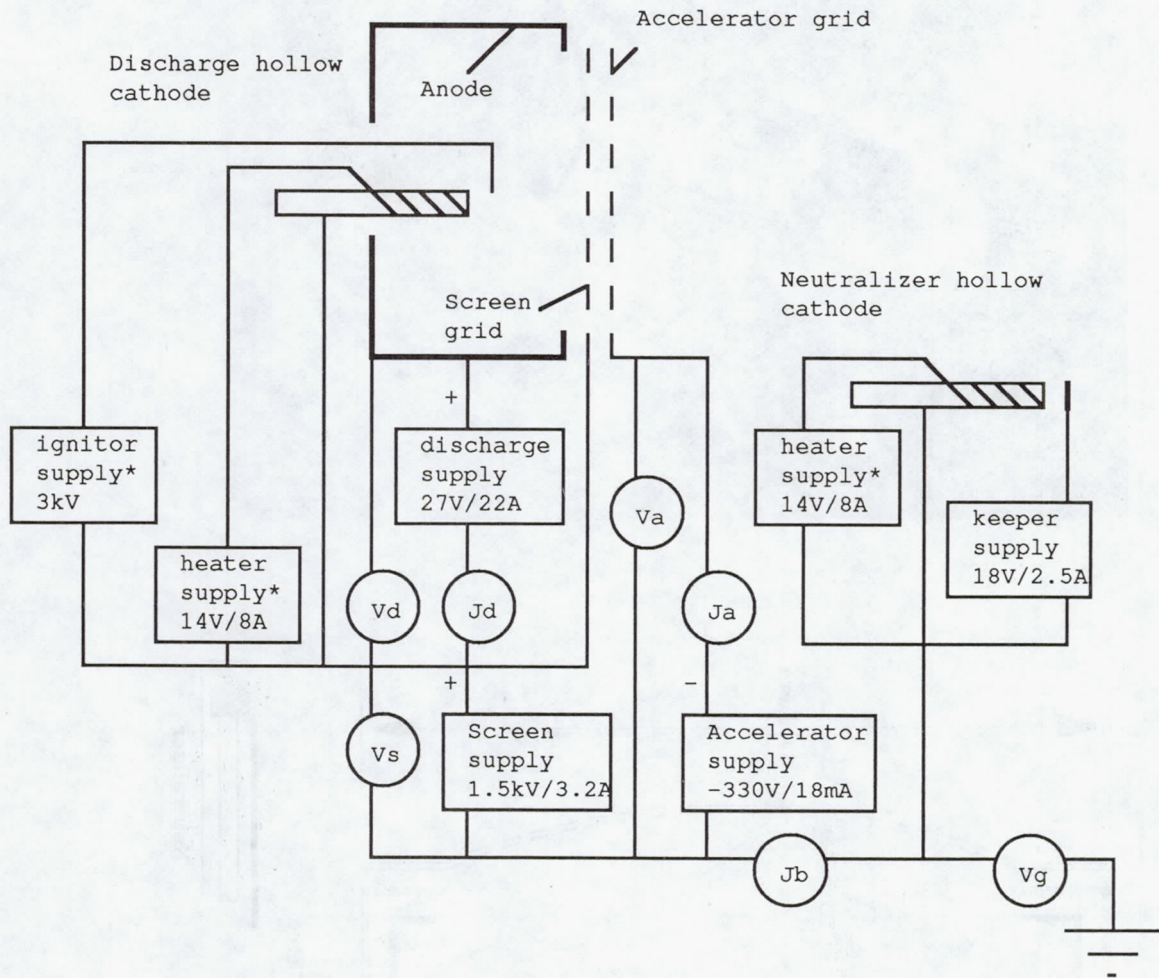
* power supplies used on start-up only

FIGURE 2. - Electrical
Schematic.

24

vacuum penetration

fluorocarbon-elastomer
propellant lines to
thruster

Xe

Ar

propellant
bottle

gas
purge
bottle

LEGEND:

○ precision leak valve

◉ cut-off valve

◍ in-line pressure gauge

▨ mass flow transducer

▧ check valve

⬚ 2-stage pressure regulator

▨ filter, 5 micron

▯ relief valve
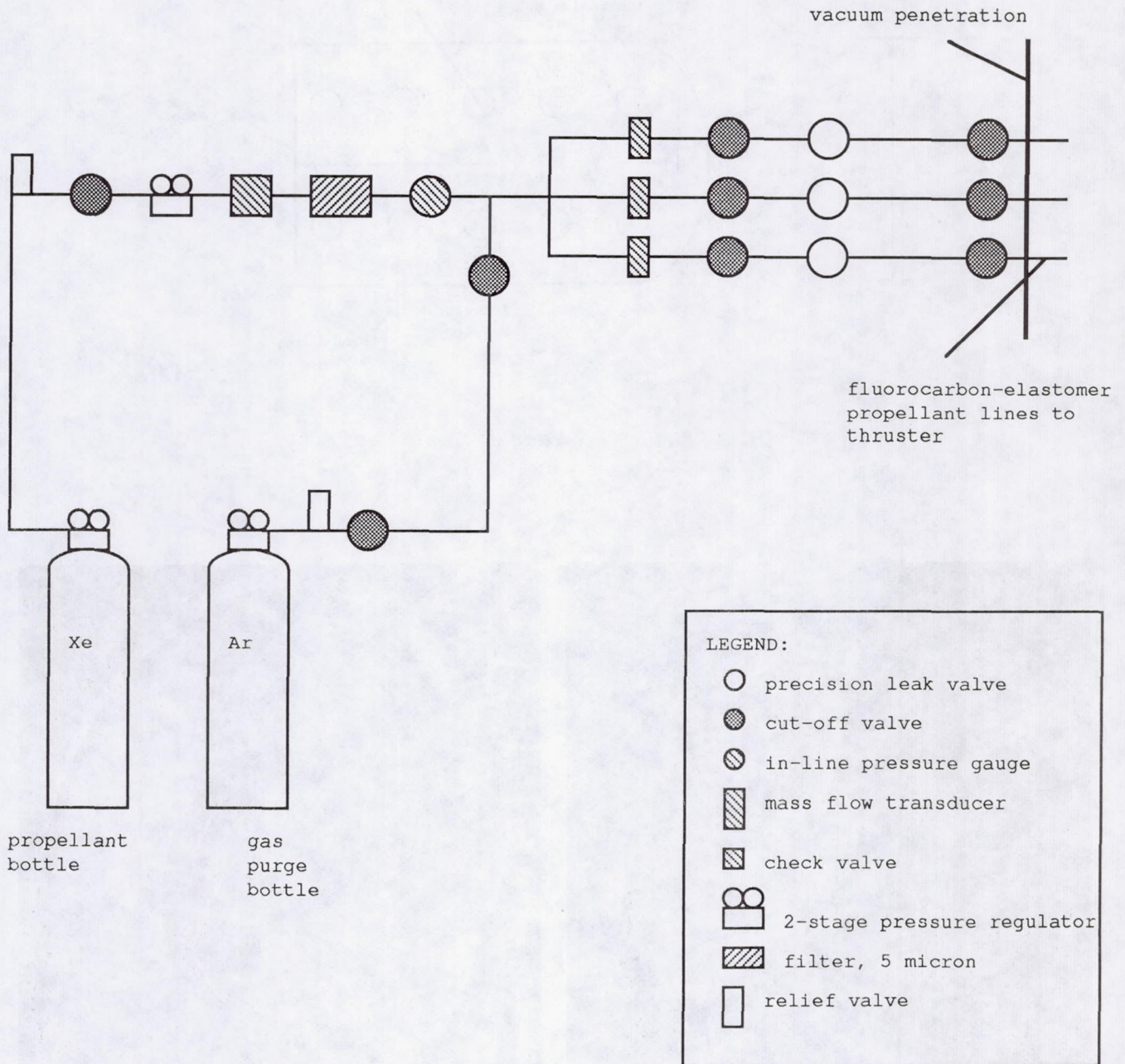
FIGURE 3. - Propellant Feed System
Schematic.
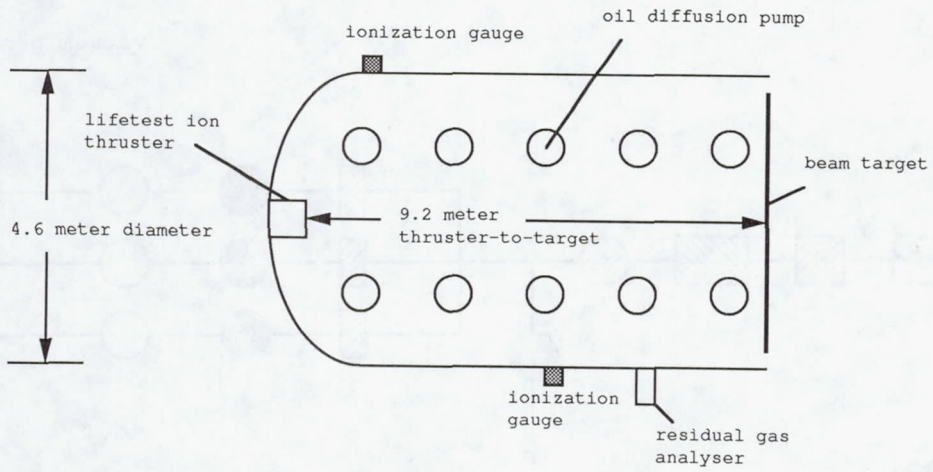
FIGURE 4. - Vacuum Test Facility
Schematic.
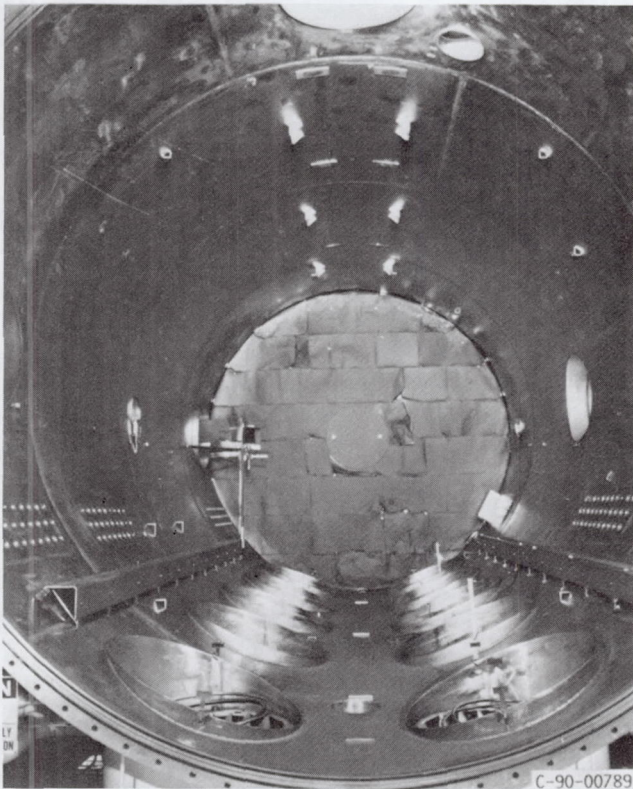
(A)   Main Chamber and Beam Target.
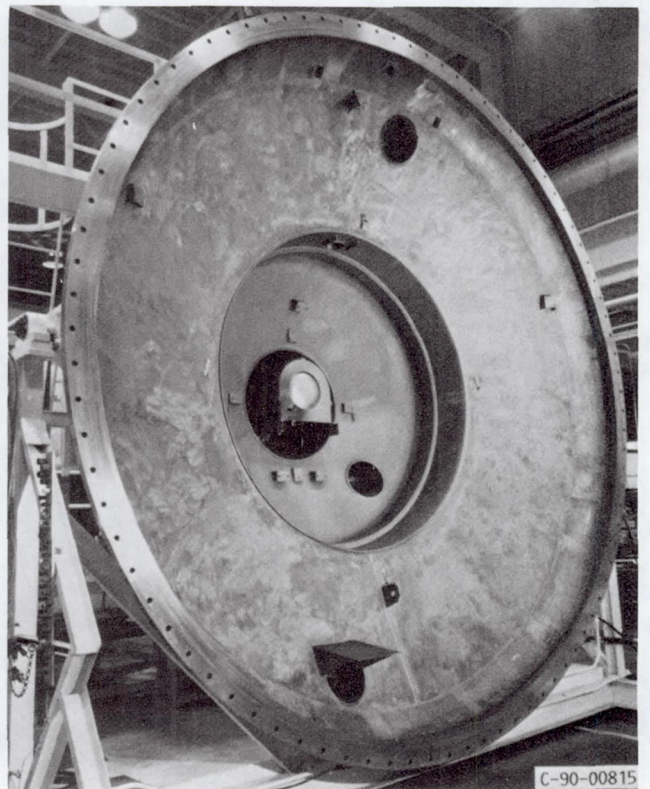
(B)   Chamber Endcap and Lifetest Thruster.

FIGURE 5. - Vacuum Test Facility.

26

EVENT #3   EVENT #6

                               317.7 hrs   576.6 hrs

LIFETEST START | | TEST TERMINATED

                          EVENT #2   EVENT #5

        EVENT #1 | | EVENT #4 | |

        184.5 hrs 291.5 hrs   441.4 hrs 572.4 hrs   890.0 hrs

  ◯━━━━━━━━━━━━━━┿━━━━━━┿┿━━━━━━━━━━━┿━━━━━━┿┿━━━━━━━━━◯

 1600 hours   ▲   ▲   625.0 hrs   1500 hrs
 12-1-89   ┌─────────────┐   1-8-90
                │ beam off   │   EVENT #7   ▲
                │ for 2 hours │
                │ to check HV │
                │ power supplies│
                └─────────────┘
                                                          ┌──────────────────────┐
                          ┌──────────────────────┐   │ propellant depletion/ │
                          │ beam and neutralizer │   │ changeout   --   and │
                          │ off for 4.5 hours to │   │ neutralizer keeper   │
                          │ repair power supply   │   │ failure on restart   │
                          └──────────────────────┘   └──────────────────────┘

NOTES:

EVENTS #2 and #4 - #7:   discharge-out on high voltage
                         recycle due to arc quenching the
                         discharge

TEST PERIOD: 910.0 hrs elapsed period
                         890.0 hrs run time
                         884.8 hrs at full power

FIGURE 6.   -   Chronology of
Events.
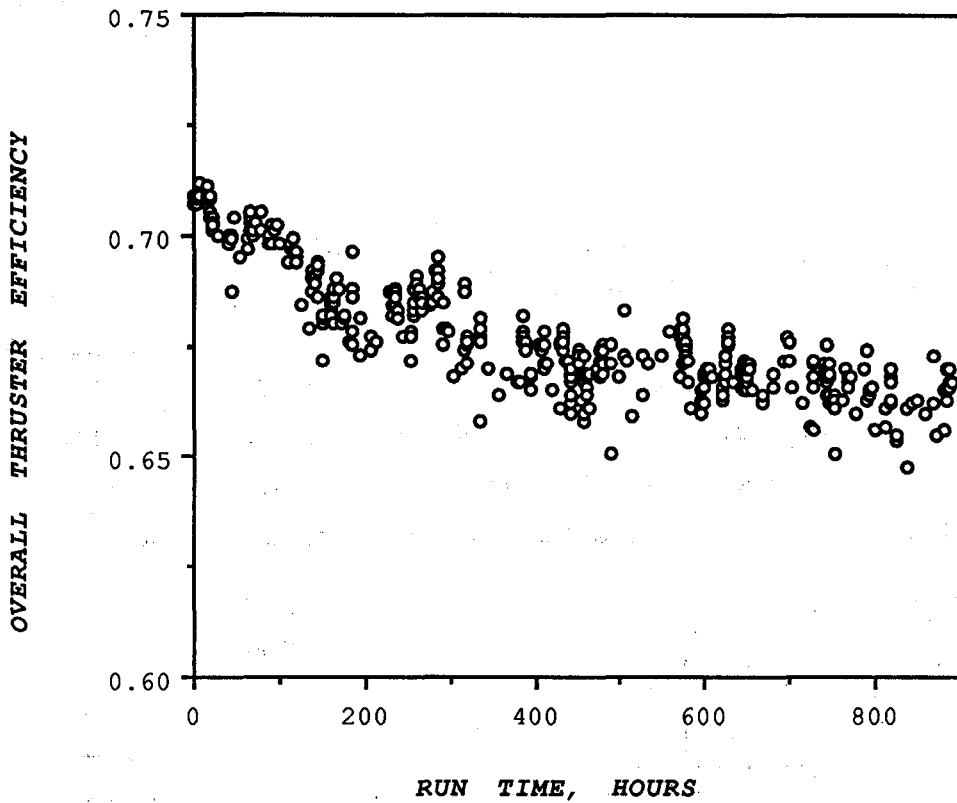
FIGURE 7. - Overall Thruster Efficiency versus Run Time.
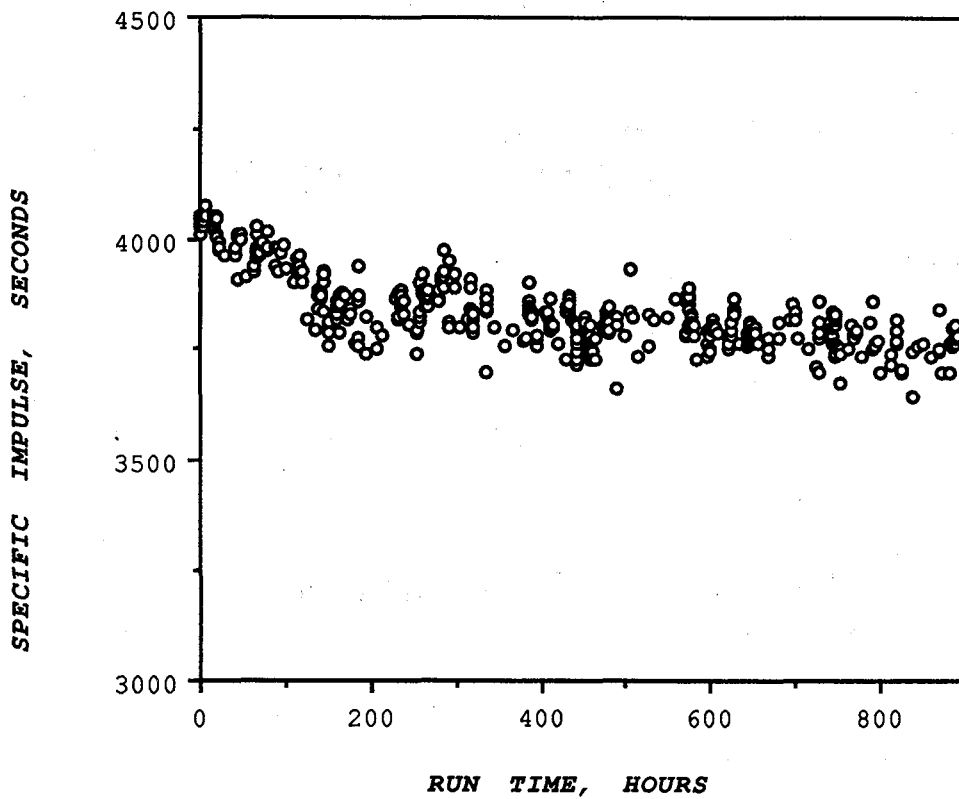
FIGURE 8. - Specific Impulse versus Run Time.

28
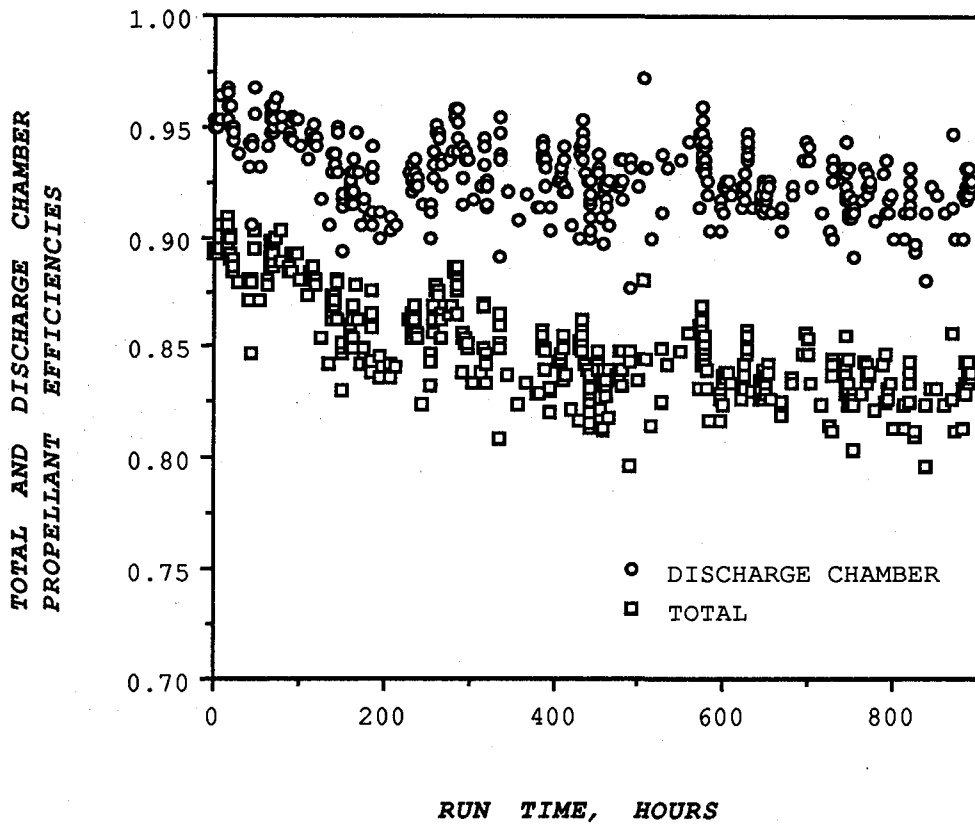
FIGURE 9. - Total and Discharge Chamber Propellant
Efficiencies versus Run Time.
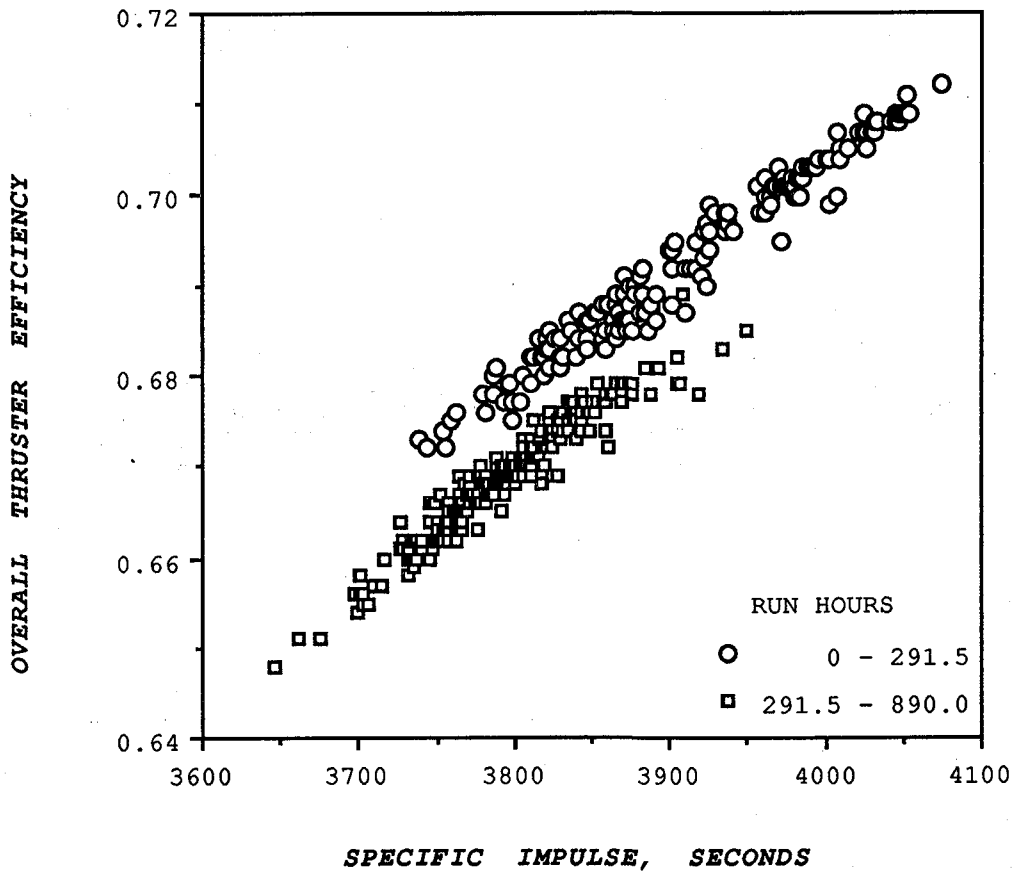
FIGURE 10. - Overall Thruster Efficiency versus
Specific Impulse, for Lifetest Duration.
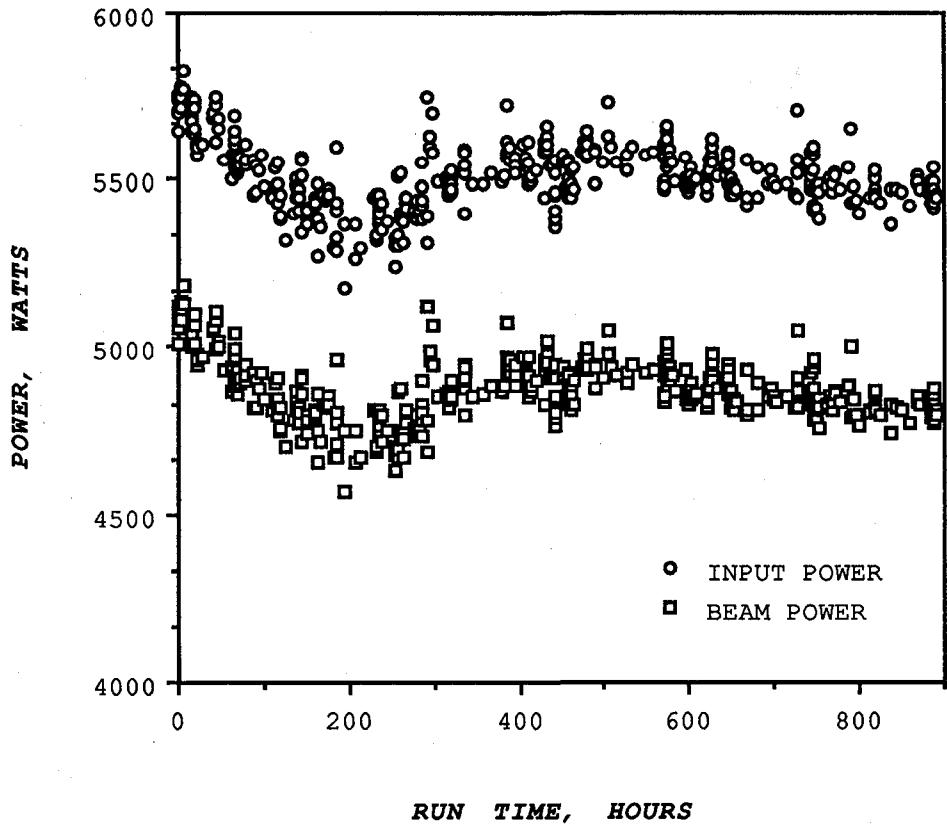
FIGURE 11. - Thruster Input and Beam Power versus Run Time.
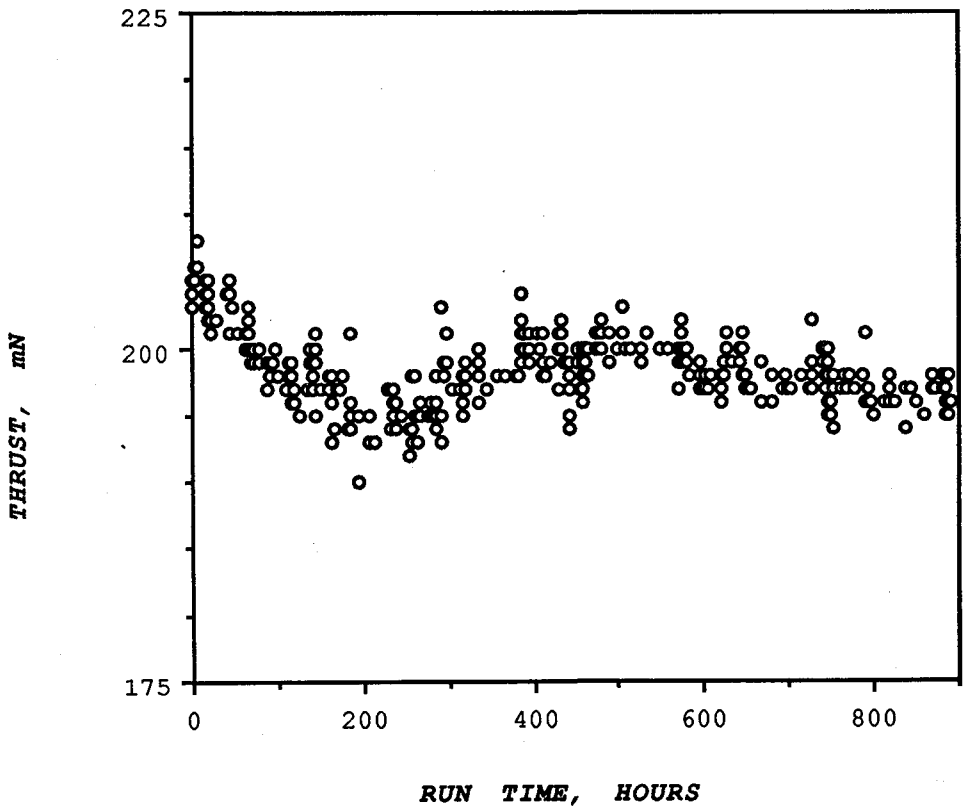
FIGURE 12. - Thrust versus Run Time.
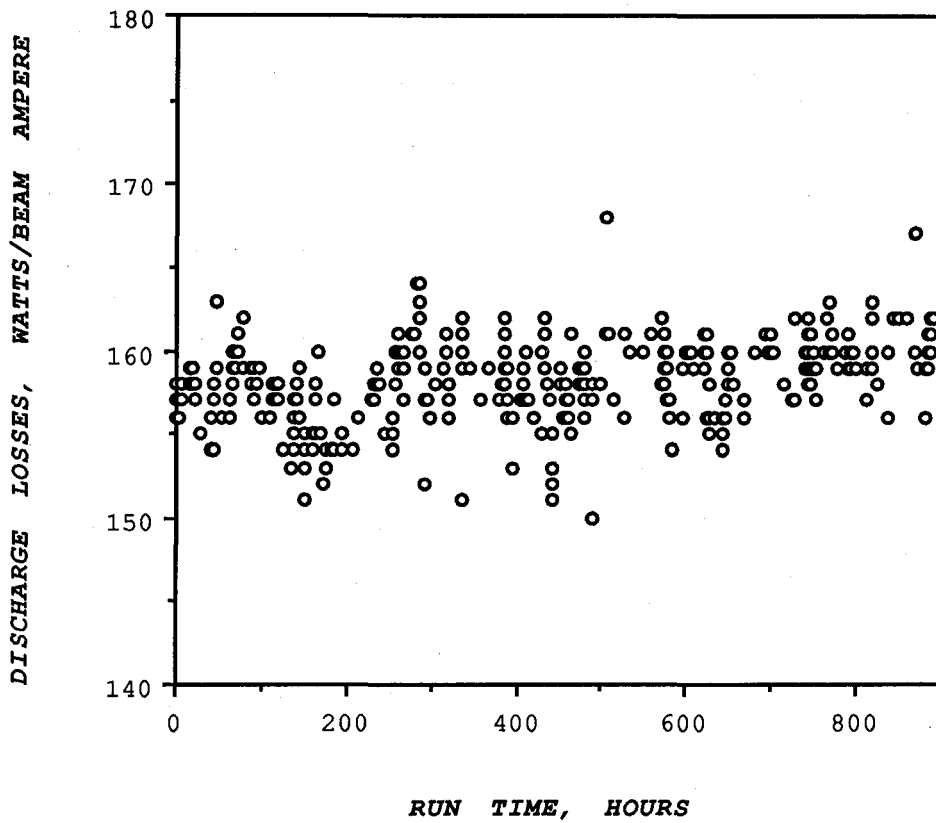
FIGURE 13. – Discharge Losses versus Run Time.
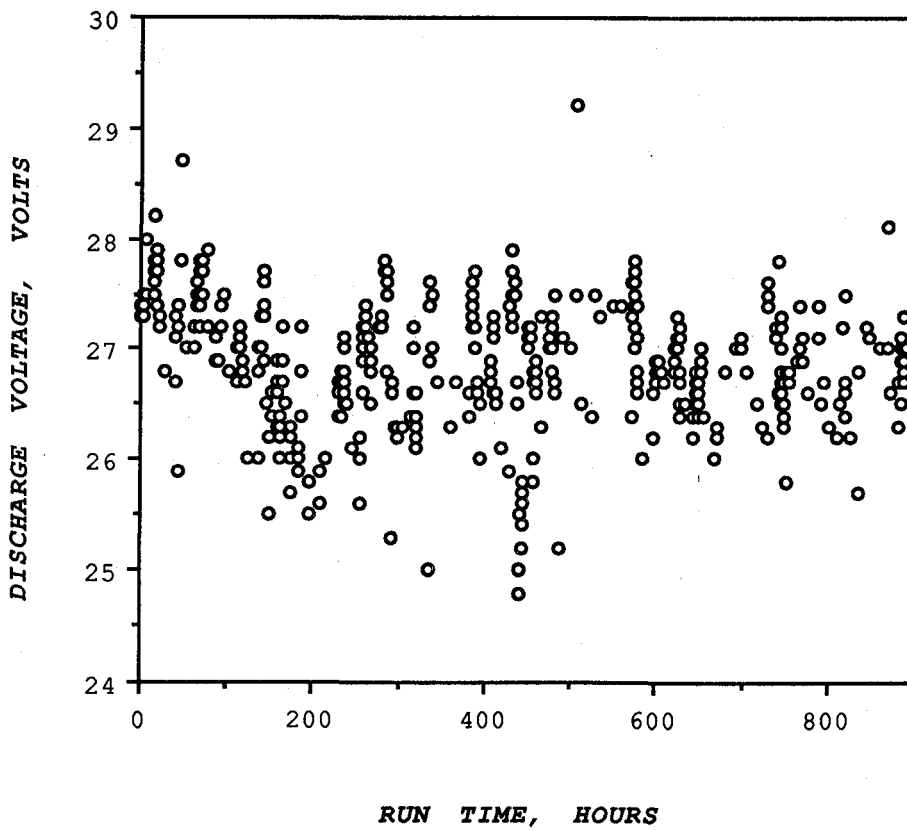
FIGURE 14. – Discharge Voltage versus Run Time.
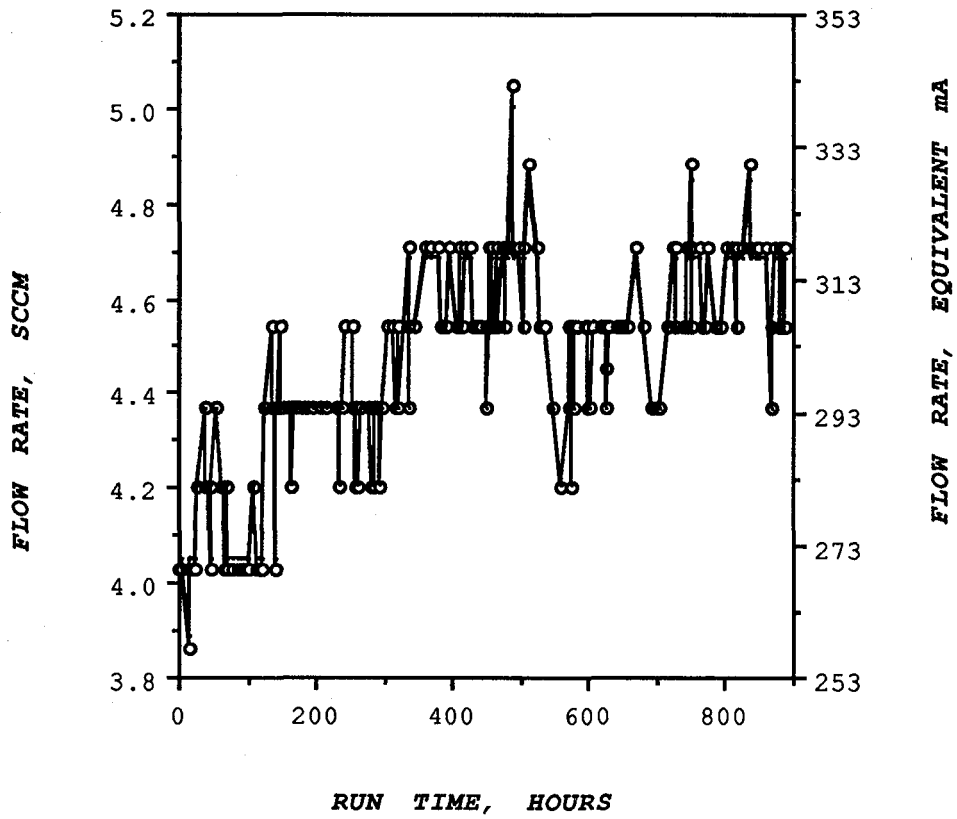
FIGURE 15. – Discharge Cathode Propellant
Mass Flow Rate versus Run Time.
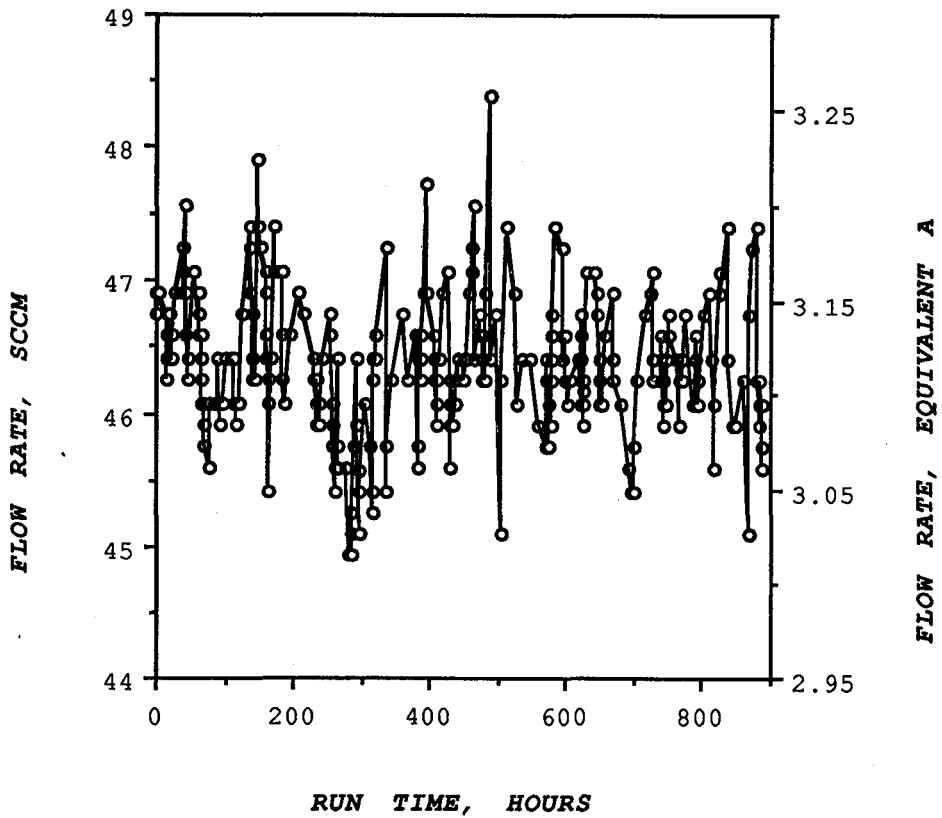
FIGURE 16. – Main Plenum Mass Flow Rate
versus Run Time.

32
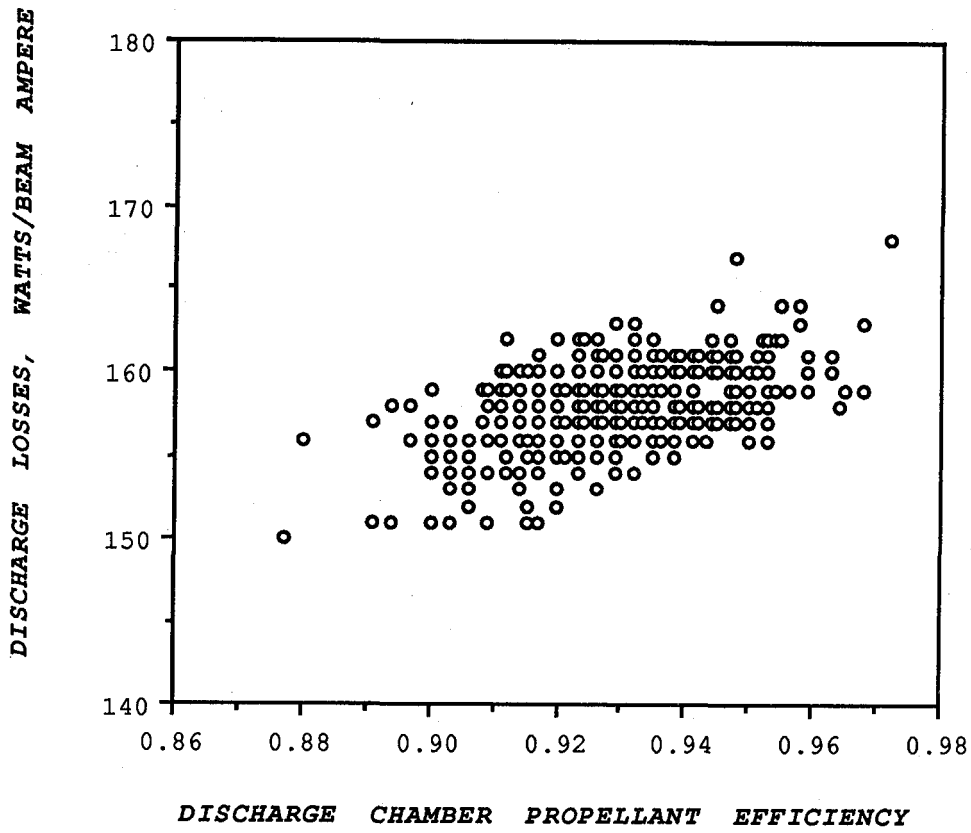
FIGURE 17. - Discharge Losses versus Discharge
Propellant Efficiency, for Lifetest Duration.
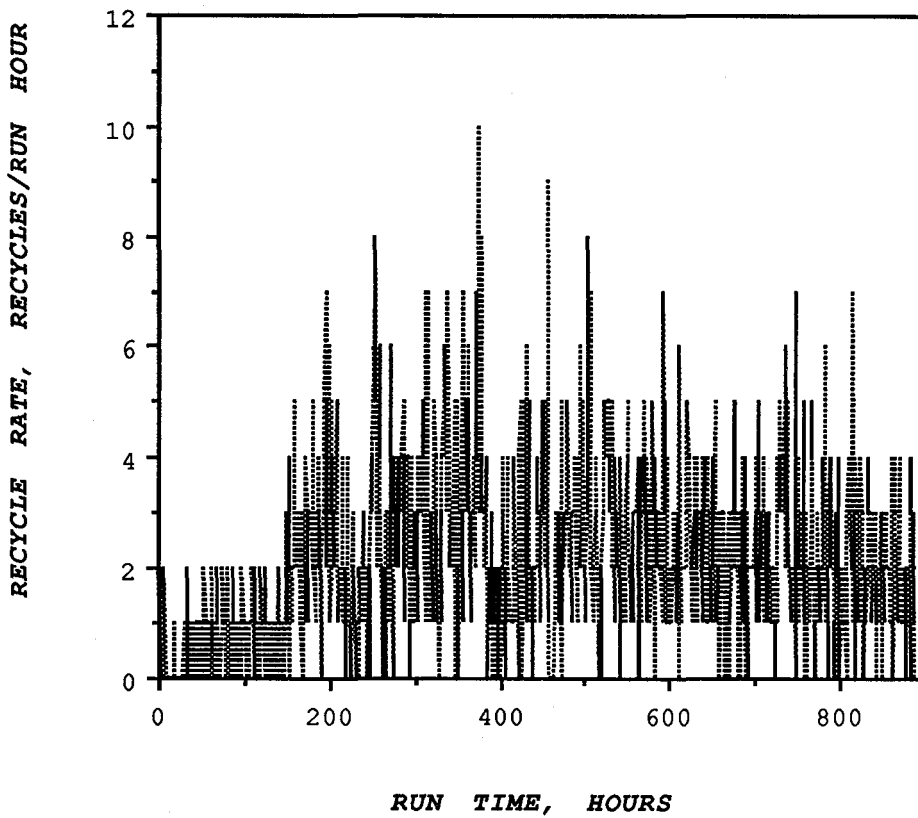
FIGURE 18A. - High-Voltage Recycle Rate
versus Run Time.
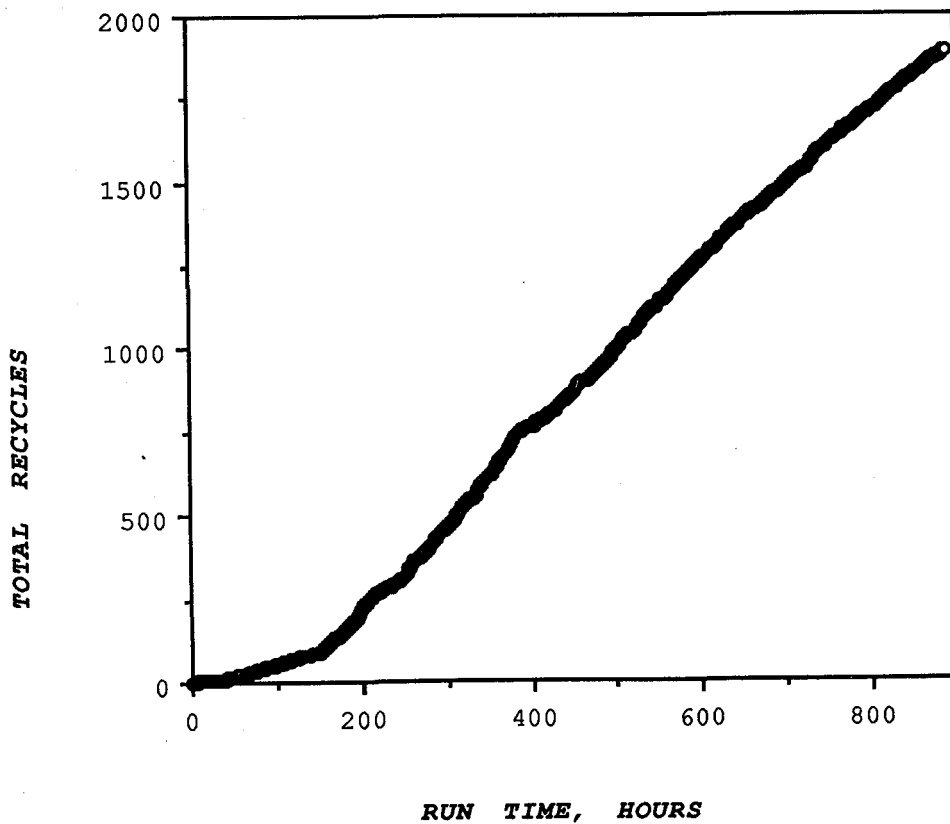
FIGURE 18B. - Cumulative Recycles versus
Run Time.
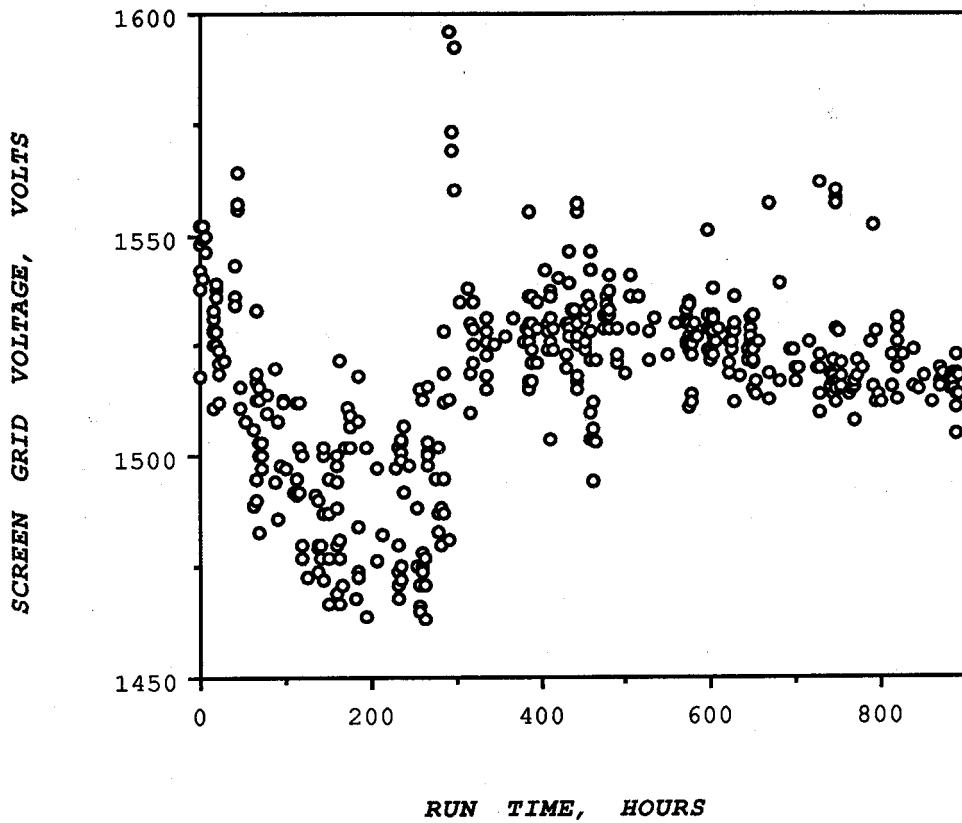
FIGURE 19. - Screen Grid Voltage versus Run Time.
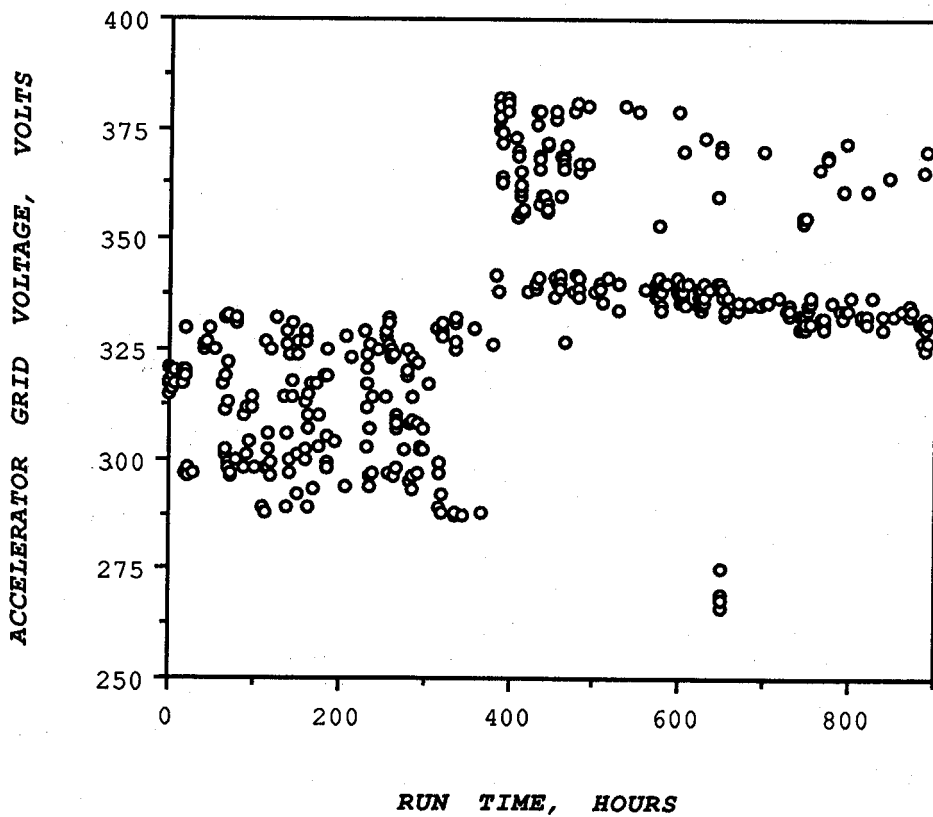
FIGURE 20. - Accelerator Grid Voltage versus Run Time.
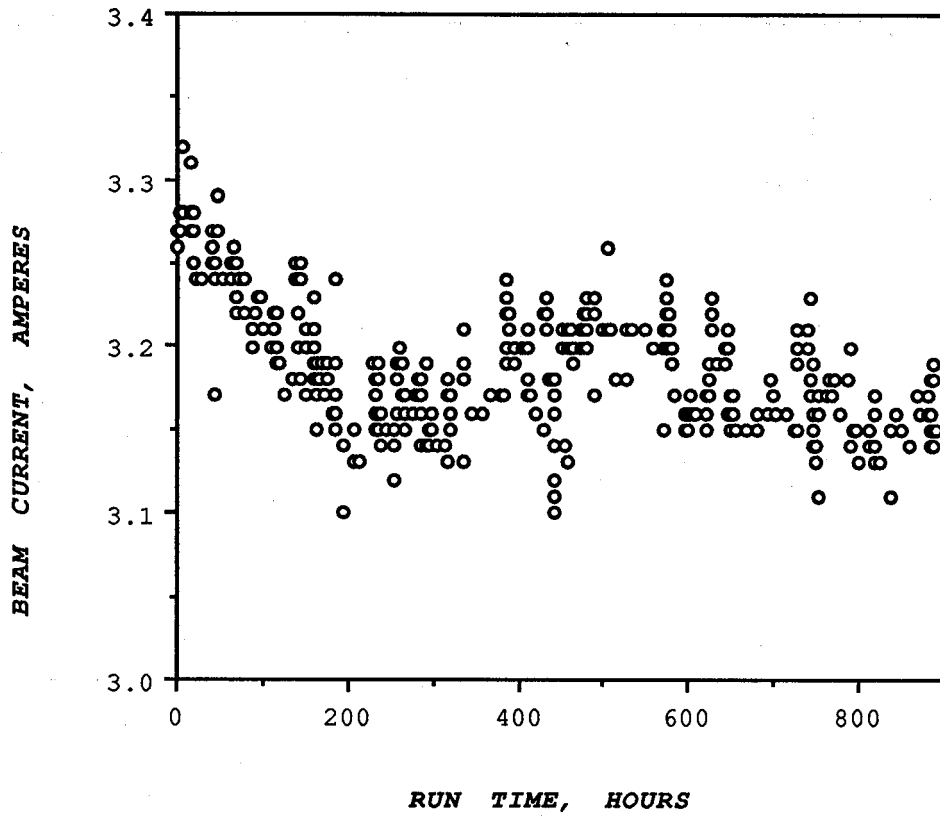
FIGURE 21. - Beam Current versus Run Time.
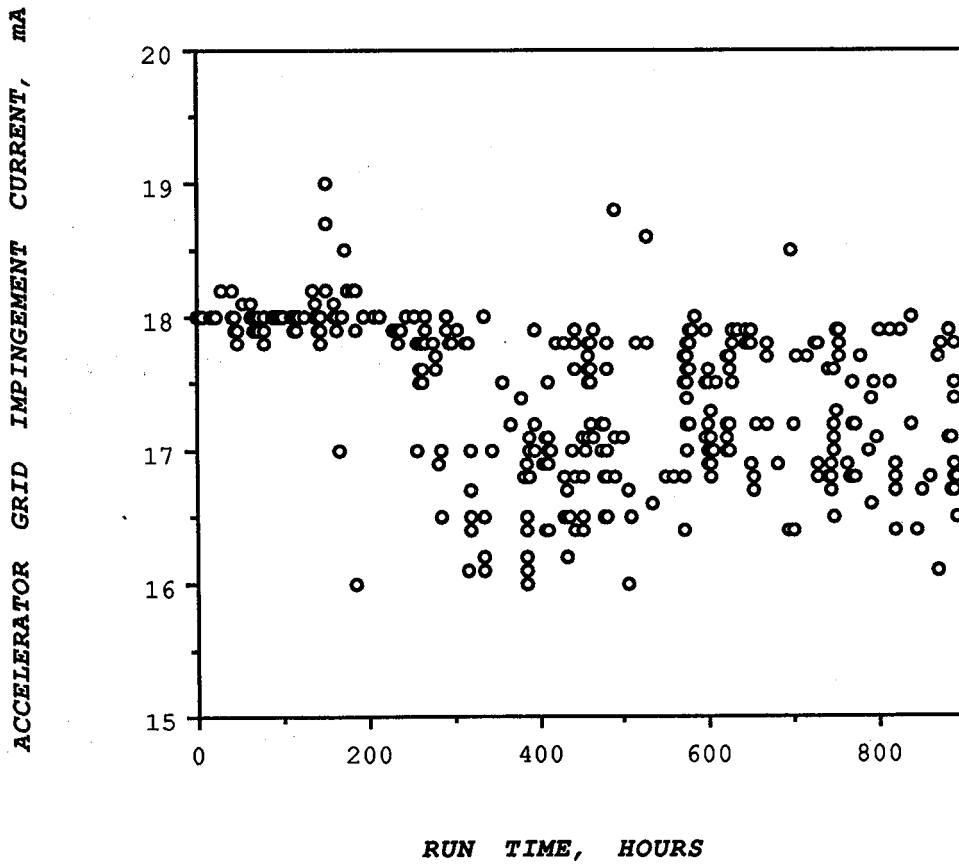
FIGURE 22. - Accelerator Grid Impingement
Current versus Run Time.

36
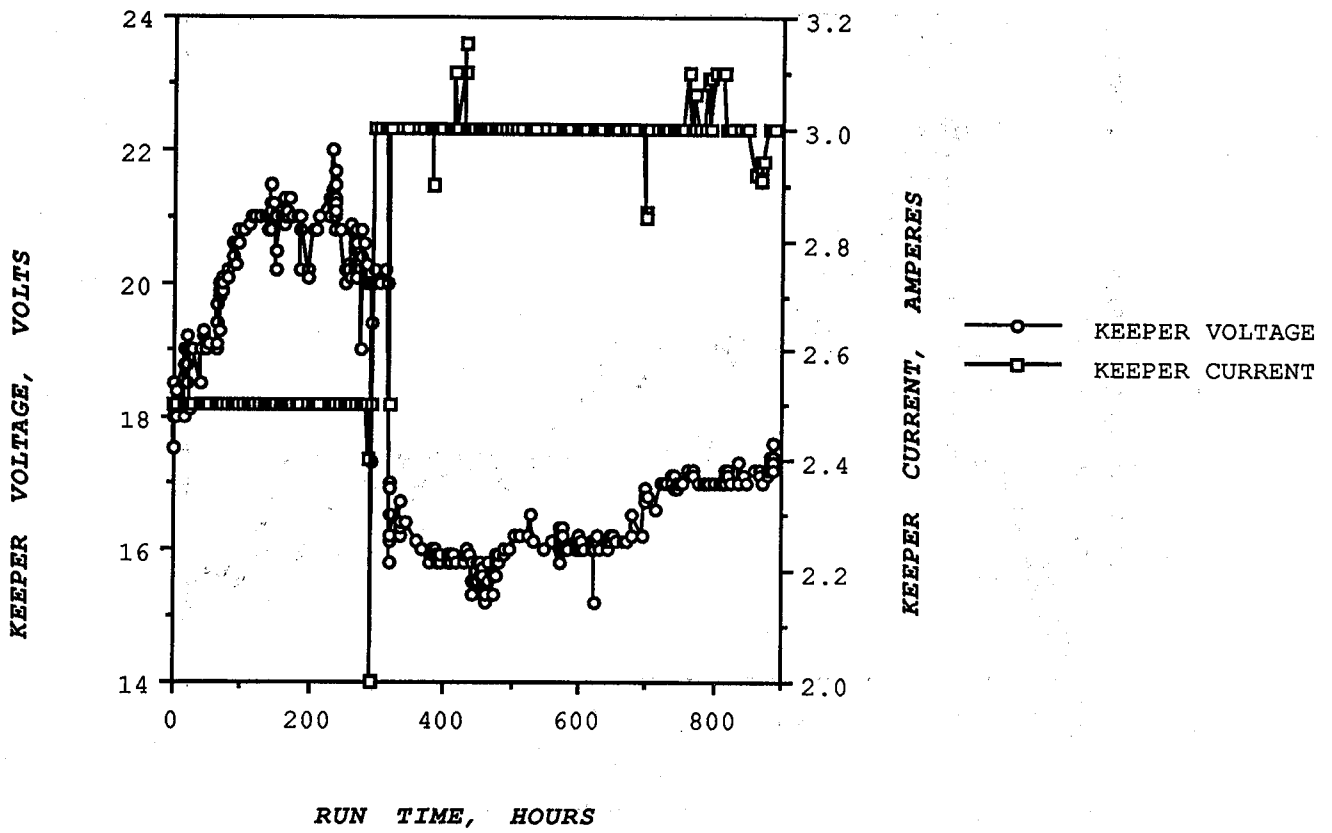
FIGURE 23. - Neutralizer Keeper Voltage
and Current versus Run Time.
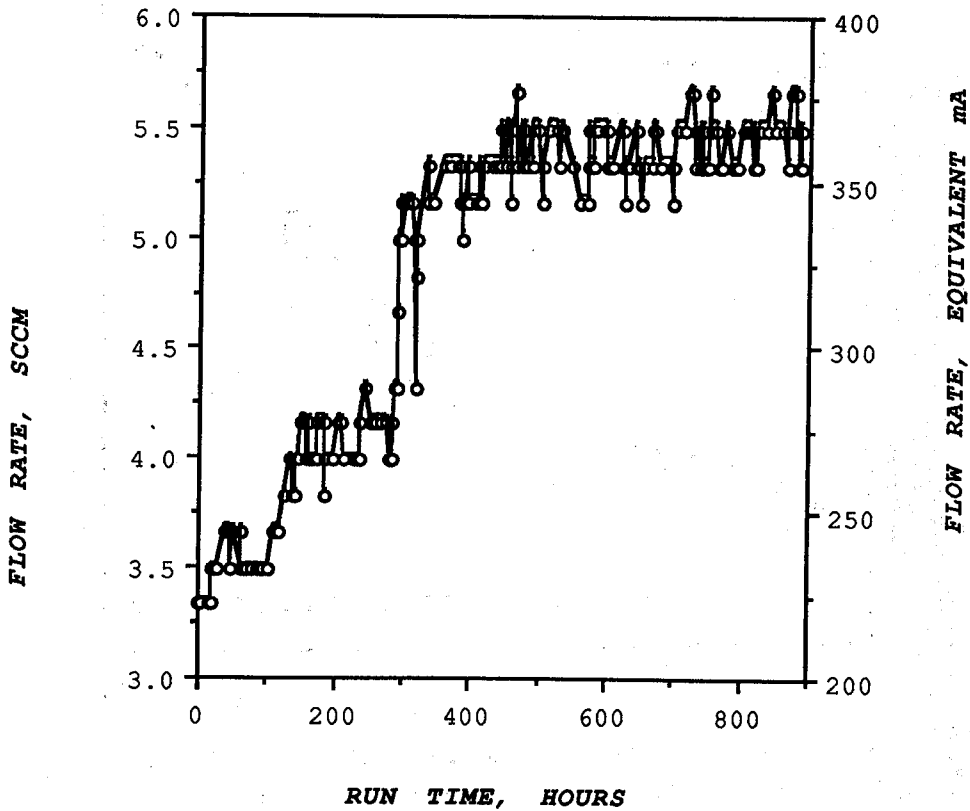
FIGURE 24. - Neutralizer Cathode Propellant
Mass Flow Rate versus Run Time.
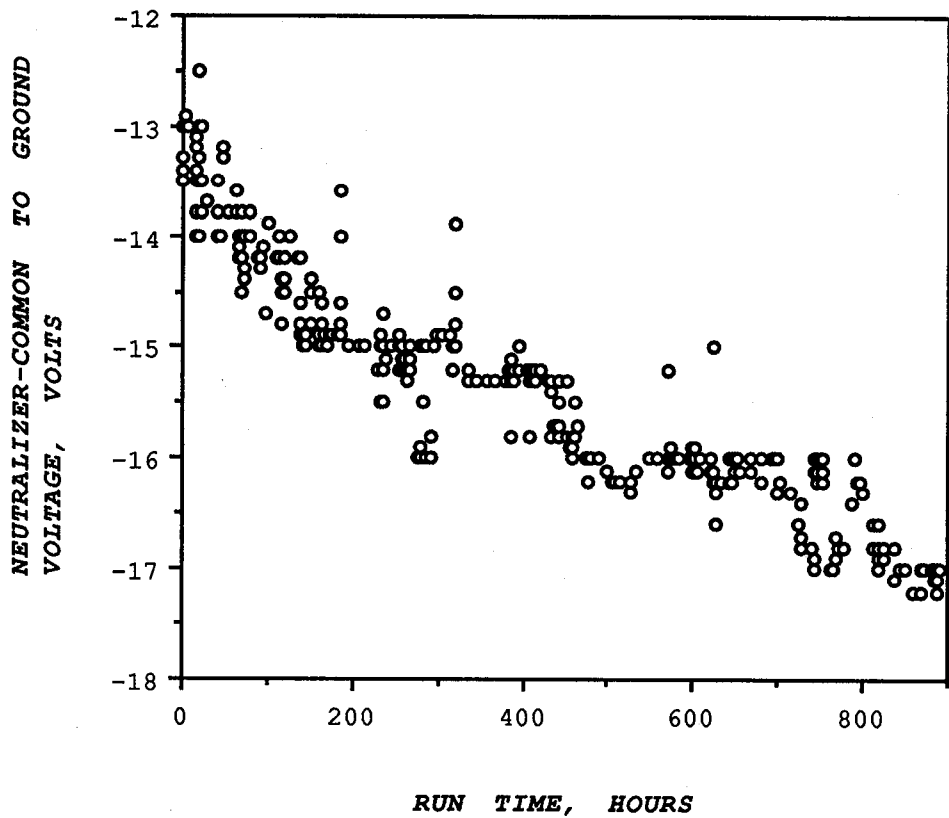
FIGURE 25. - Neutralizer-Common to Ground Voltage versus Run Time.

4.0/47 SCCM CATHODE/MAIN FLOW SPLIT

DISCHARGE CHAMBER PROPELLANT EFFICIENCY
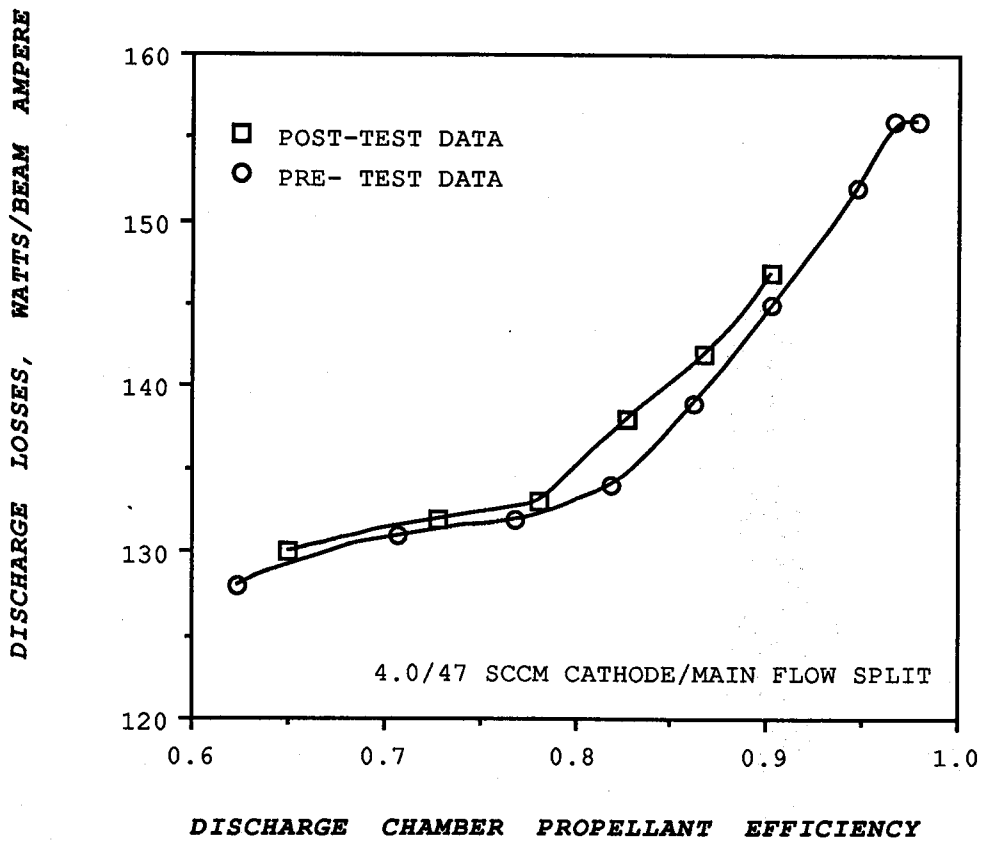
FIGURE 26. - Discharge Losses versus Propellant Efficiency, Pre- and Post-Lifetest Comparison.

38
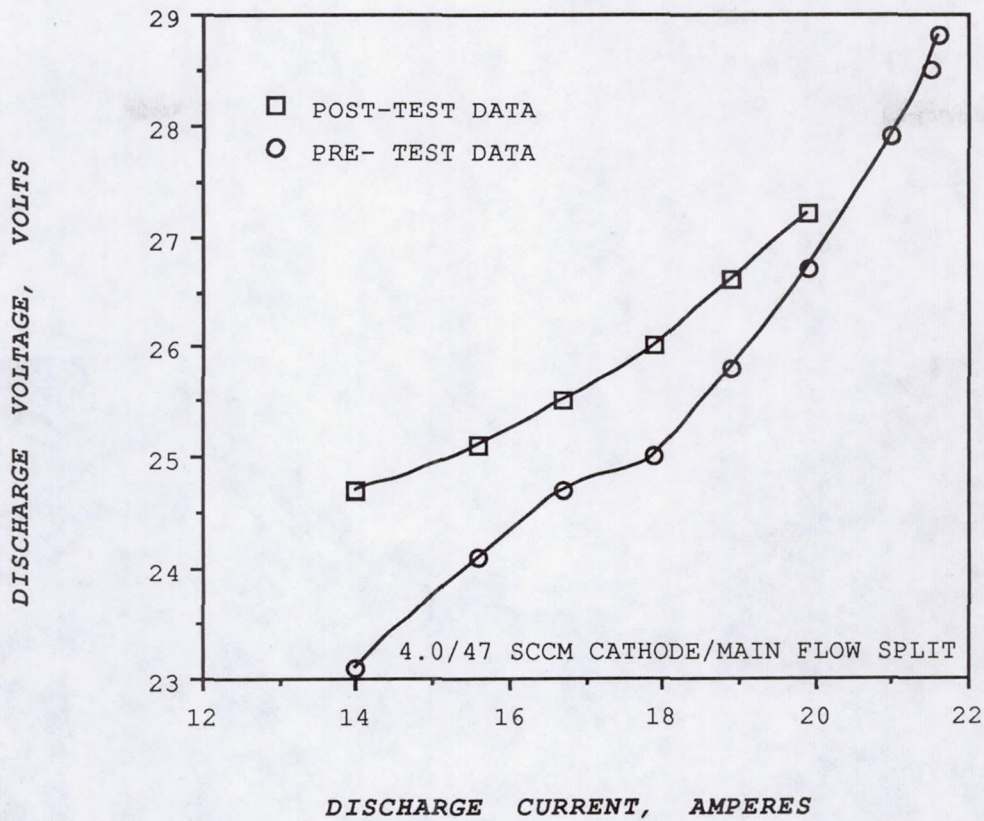
FIGURE 27. - Discharge IV Characteristic,
Pre- and Post-Lifetest Comparison.
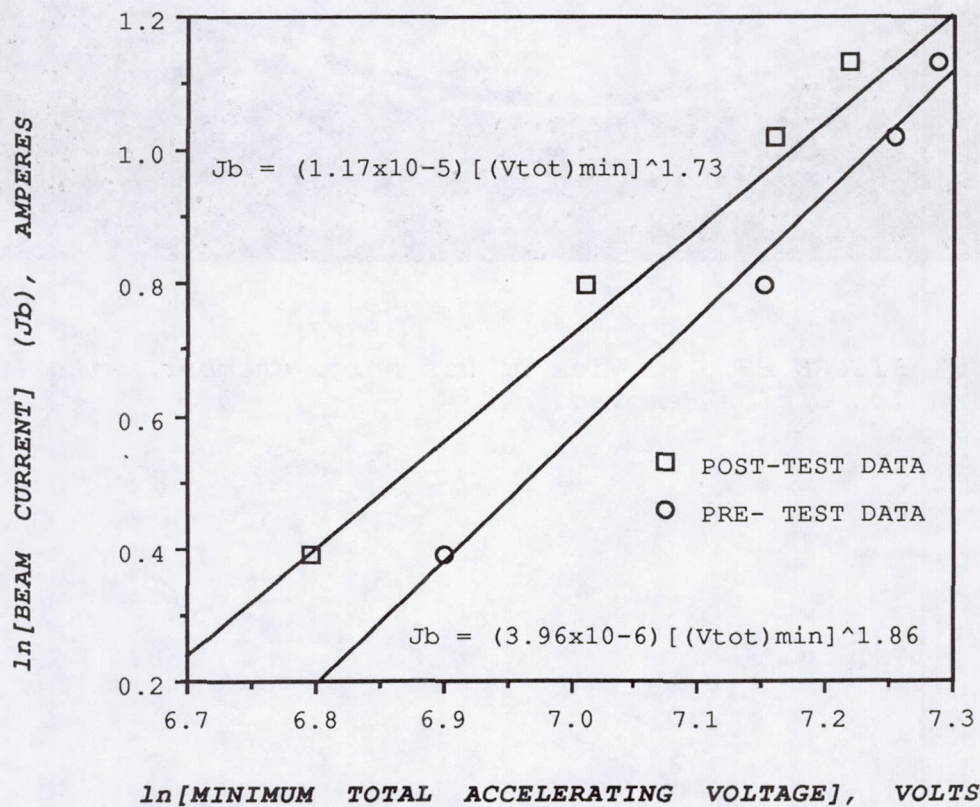
FIGURE 28. - Ion Optics Perveance,
Pre- and Post-Lifetest Comparison.

C-90-00817
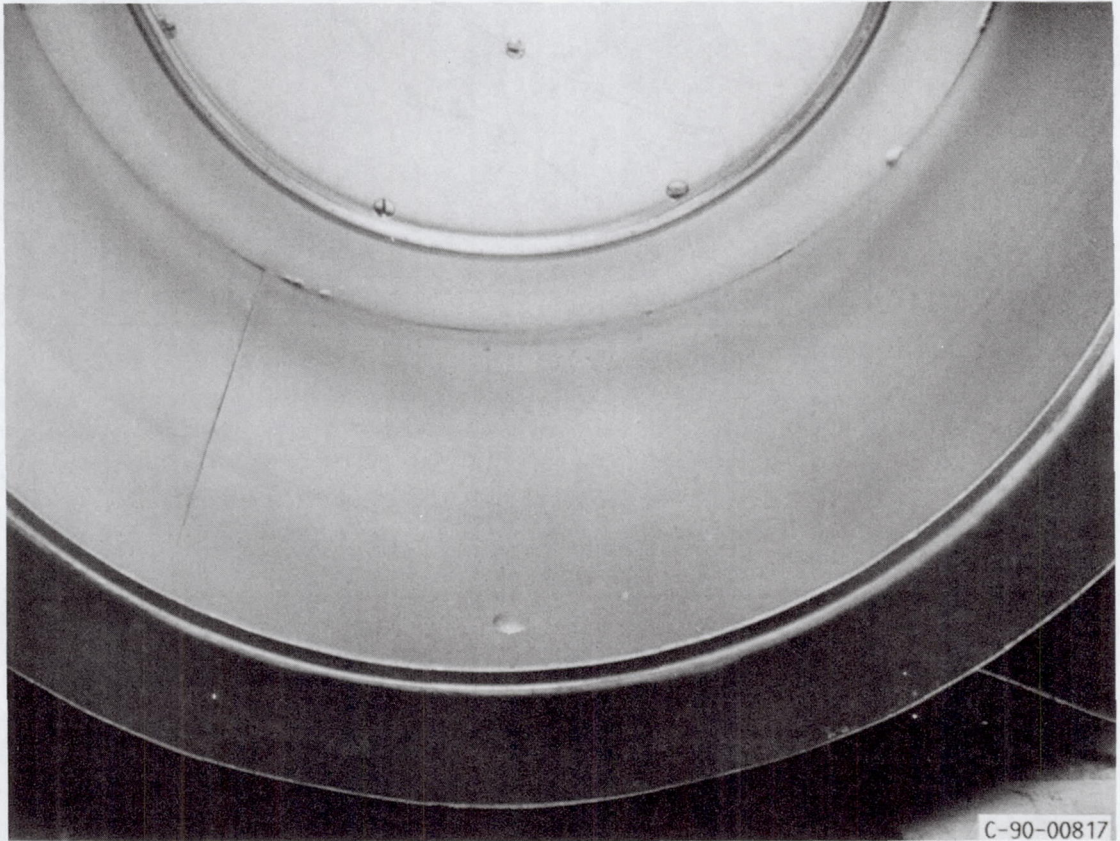
FIGURE 29.   -   View of Discharge Chamber, with
Ion Optics Removed.
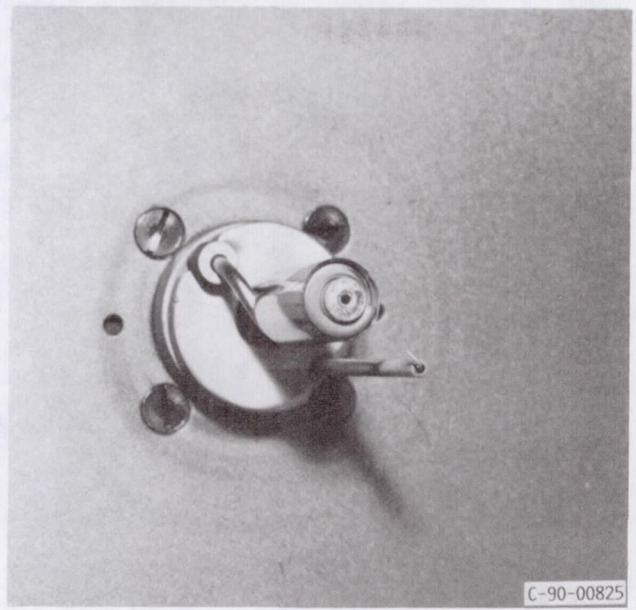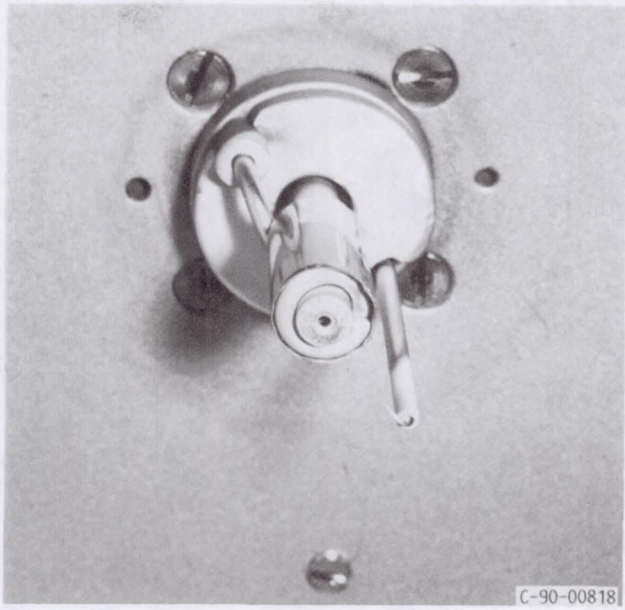
(A) and (B)   Installed in Thruster.
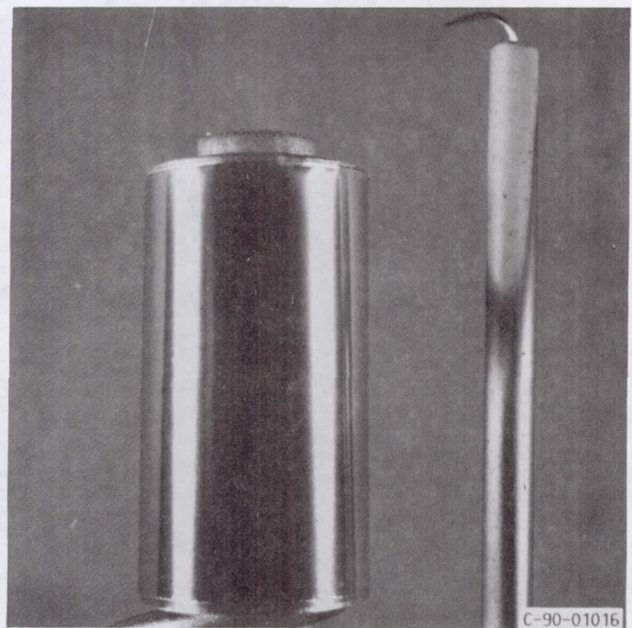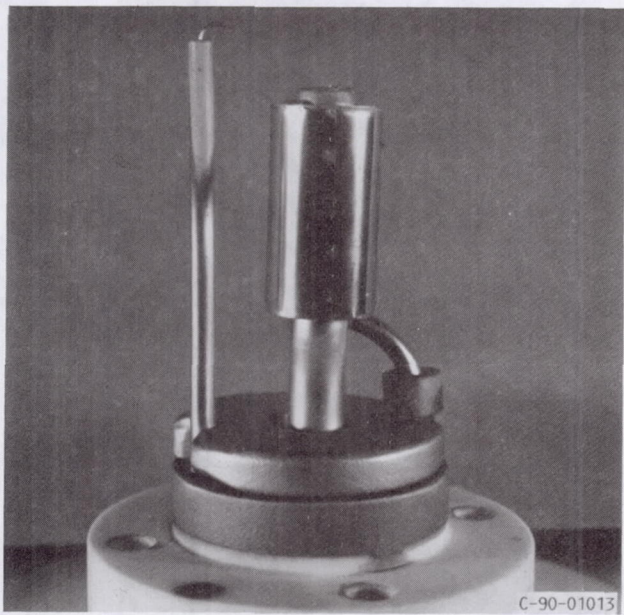
(C) and (D)   Removed from Thruster.

FIGURE 30.   - Post-Lifetest Discharge Cathode
Assembly, Several Perspectives.

41
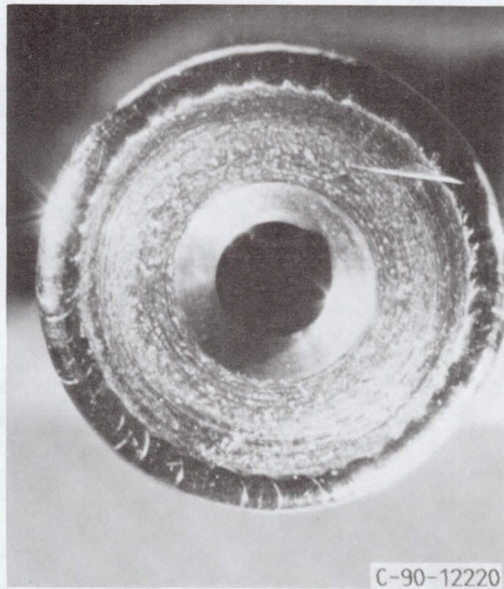
(A)   Pre-Lifetest.

(B)   Post-Lifetest.

FIGURE 31. – Discharge Cathode Orifice Plate.
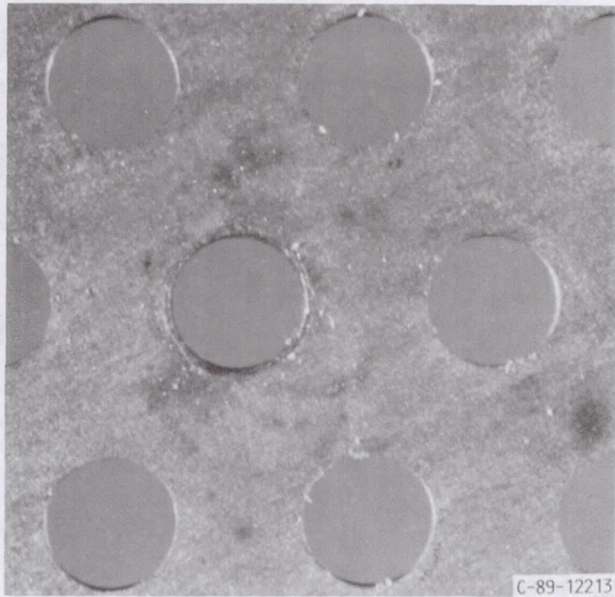
(A)   Upstream Surface, Pre-Lifetest.   (B)   Upstream Surface, Post-Lifetest.
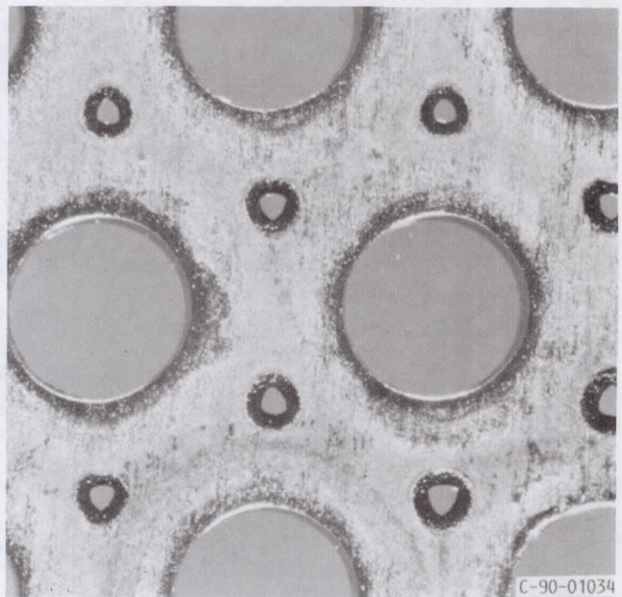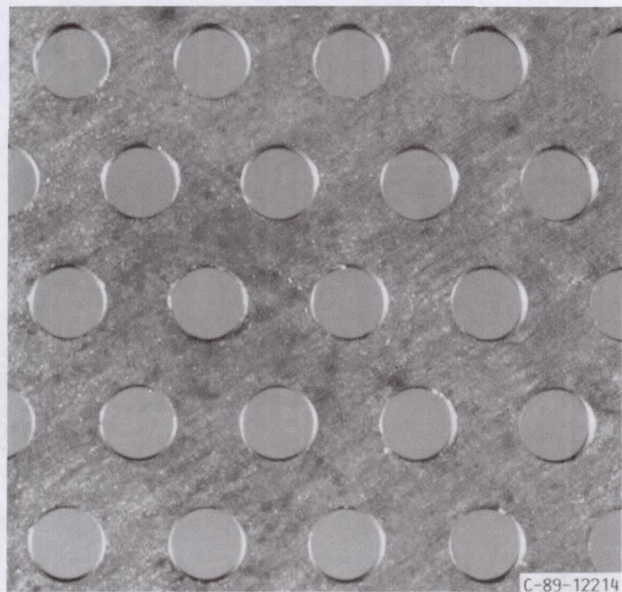
(C)   Downstream Surface, Pre-Lifetest.   (D)   Downstream Surface, Post-Lifetest.
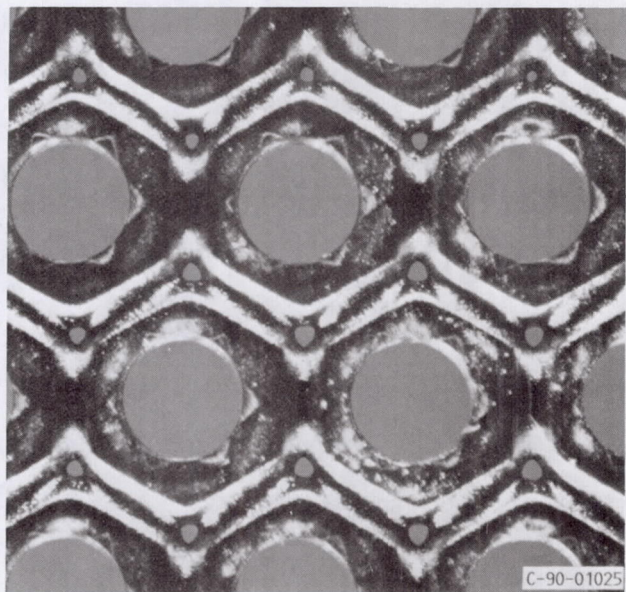
FIGURE 32. - Accelerator Grid, Center Holes.
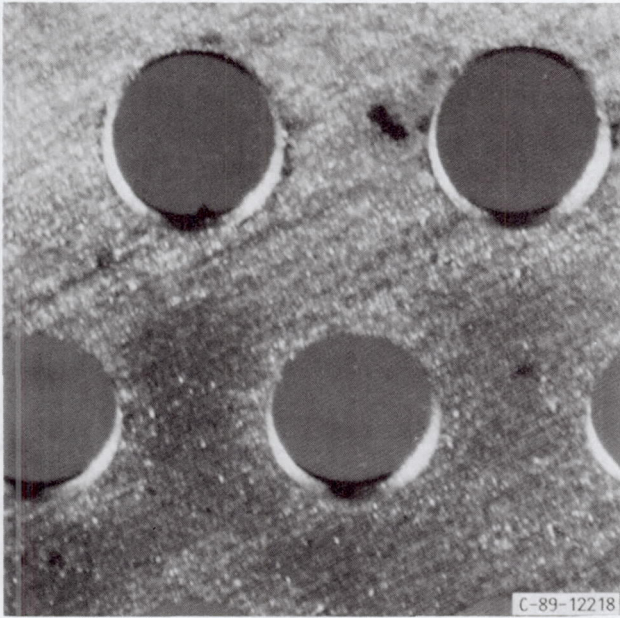
(A)   Upstream Surface, Pre-Lifetest.
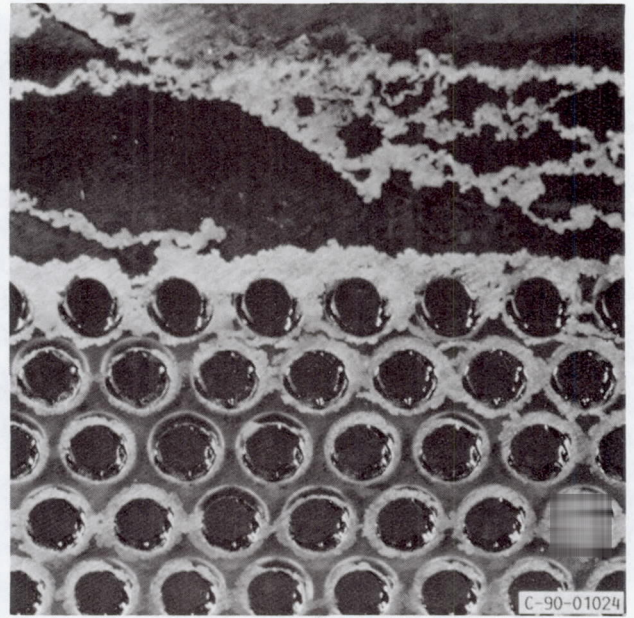
(B)   Upstream Surface, Post-Lifetest.
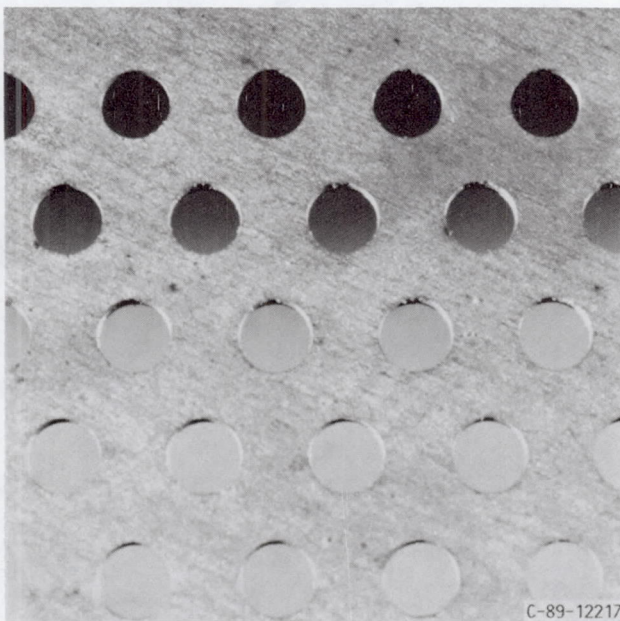
(D)   Downstream Surface, Post-Lifetest.
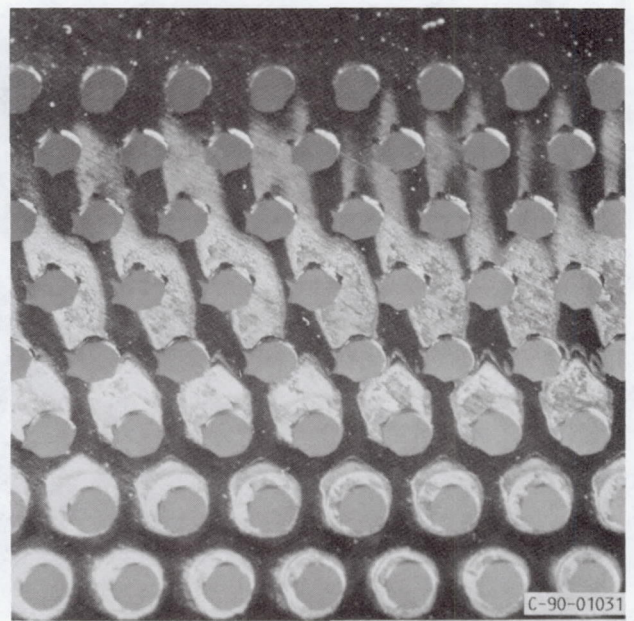
(C)   Downstream Surface, Pre-Lifetest.

FIGURE 33. - Accelerator Grid, Edge Holes.
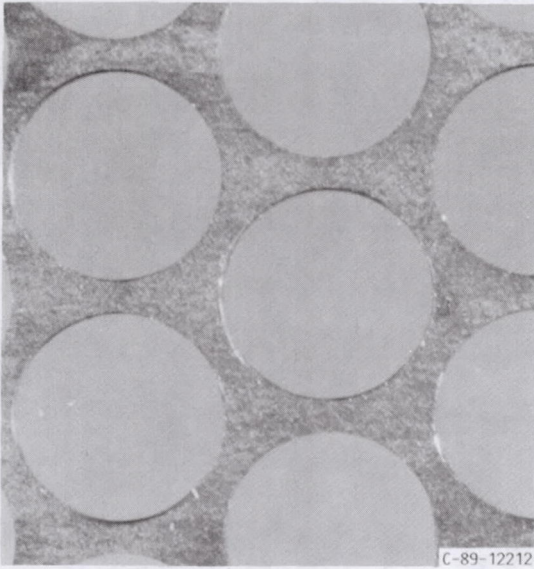
(A)   Upstream Surface, Pre-Lifetest.   (B)   Upstream Surface, Post-Lifetest.
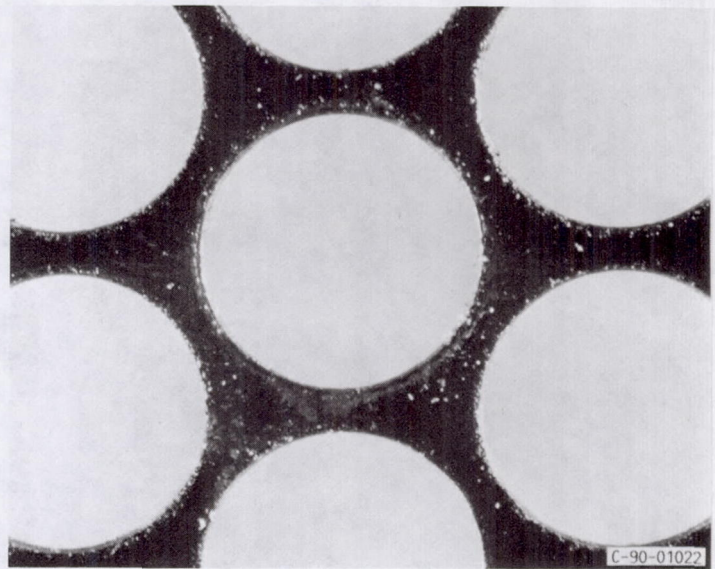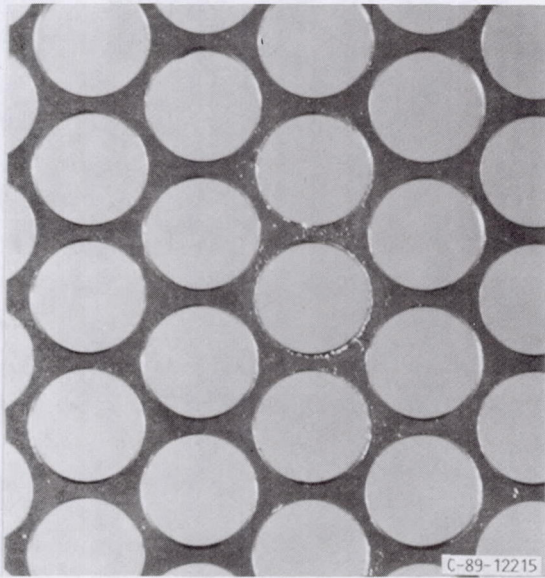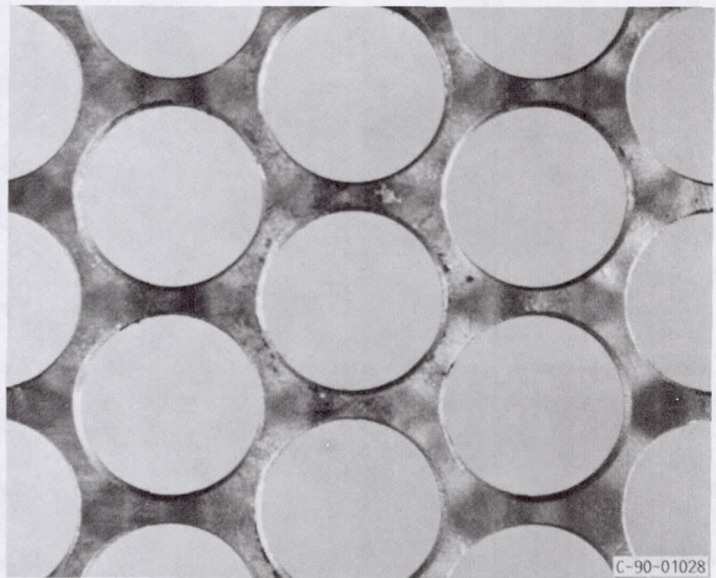
(C)   Downstream Surface, Pre-Lifetest.   (D)   Downstream Surface, Post-Lifetest.

FIGURE 34.   -   Screen Grid, Center Holes.
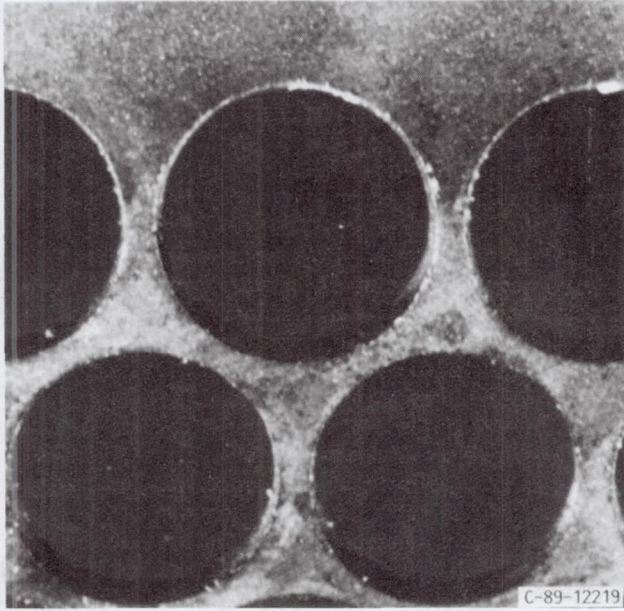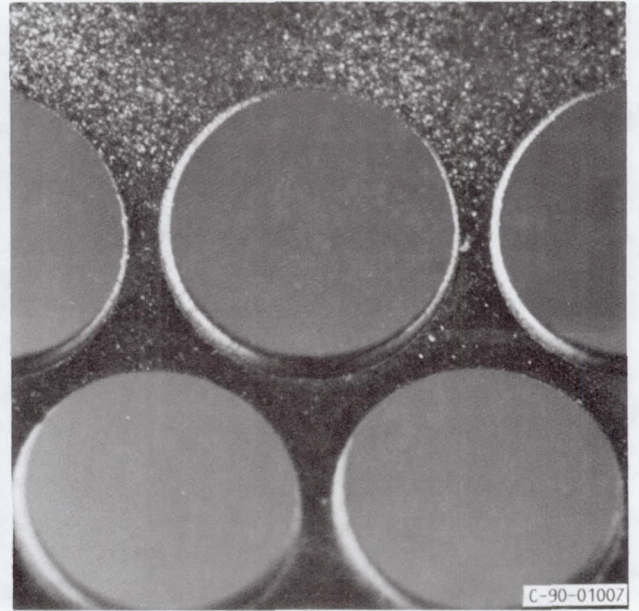
(A)   Upstream Surface, Pre-Lifetest.

(B)   Upstream Surface, Post-Lifetest.
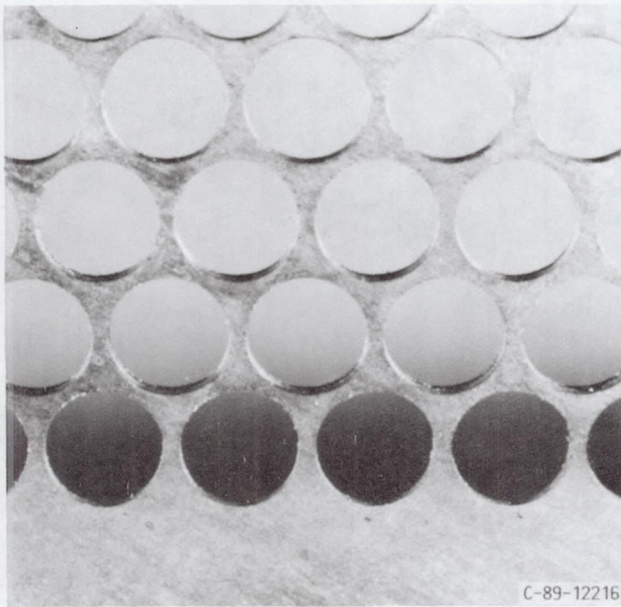
(C)   Downstream Surface, Pre-Lifetest.
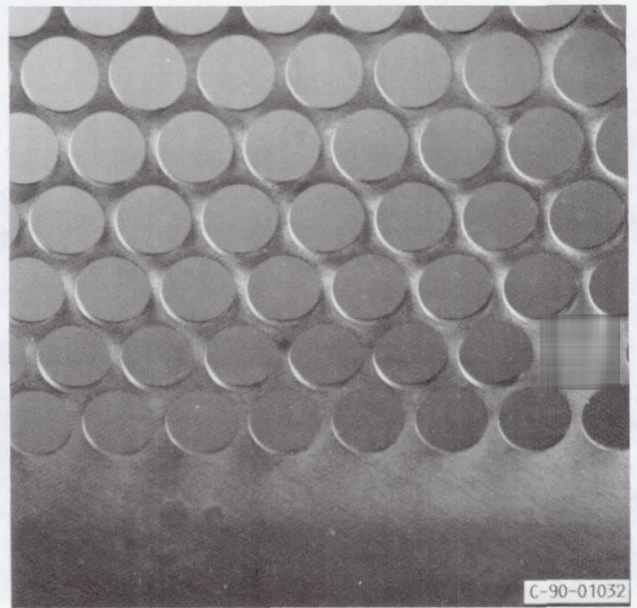
(D)   Downstream Surface, Post-Lifetest.

FIGURE 35. - Screen Grid, Edge Holes.
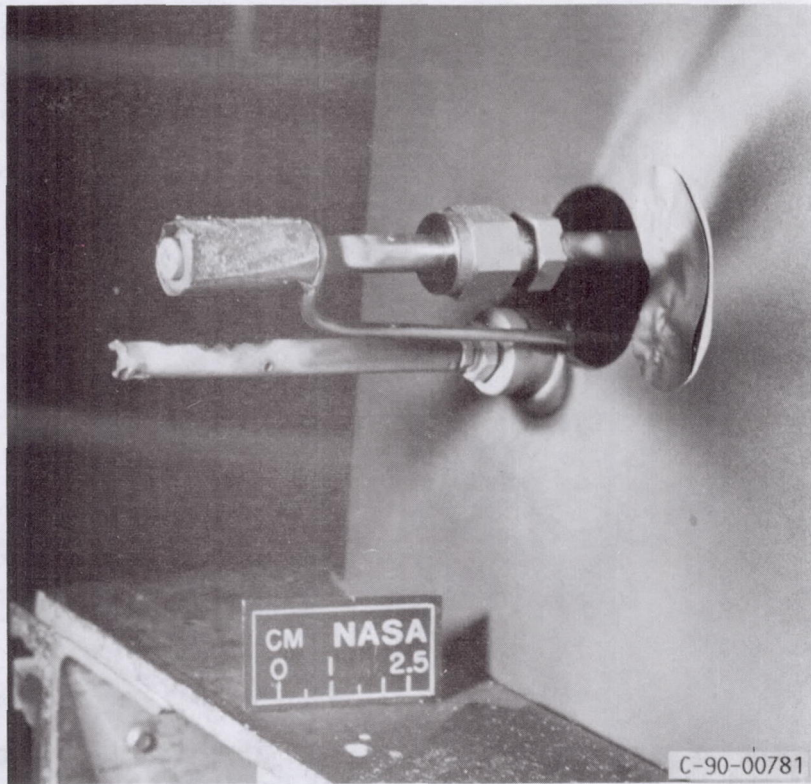
(A)   Installed on Thruster.
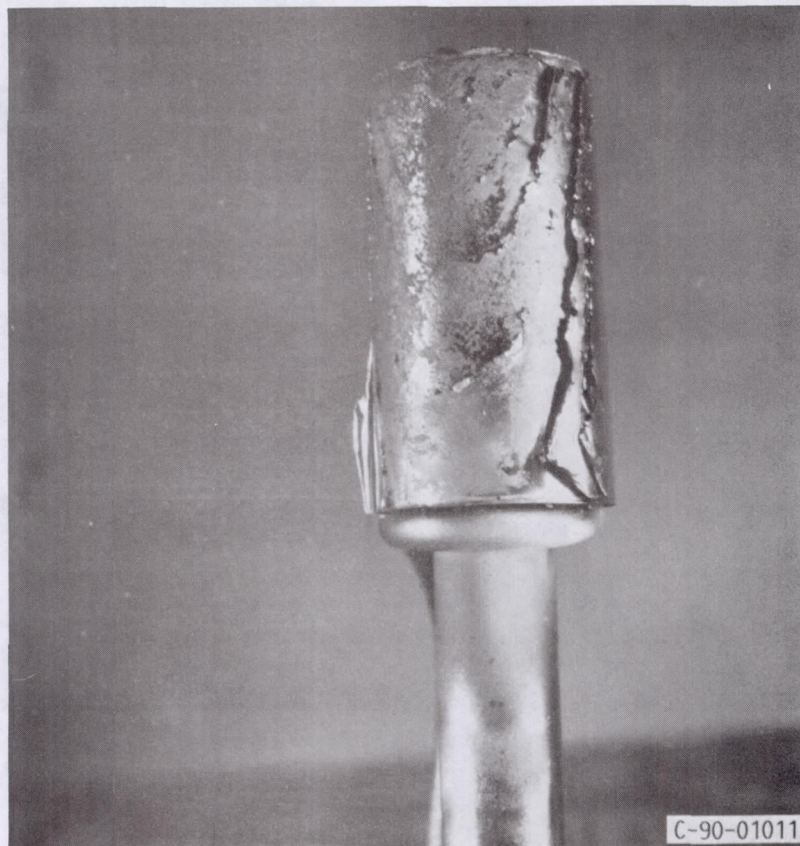
(B)   Removed from Thruster.

FIGURE 36. - Post-Lifetest Neutralizer Cathode
Assembly, Evidence of Beam Interception.

47

(A)   Pre-Lifetest.
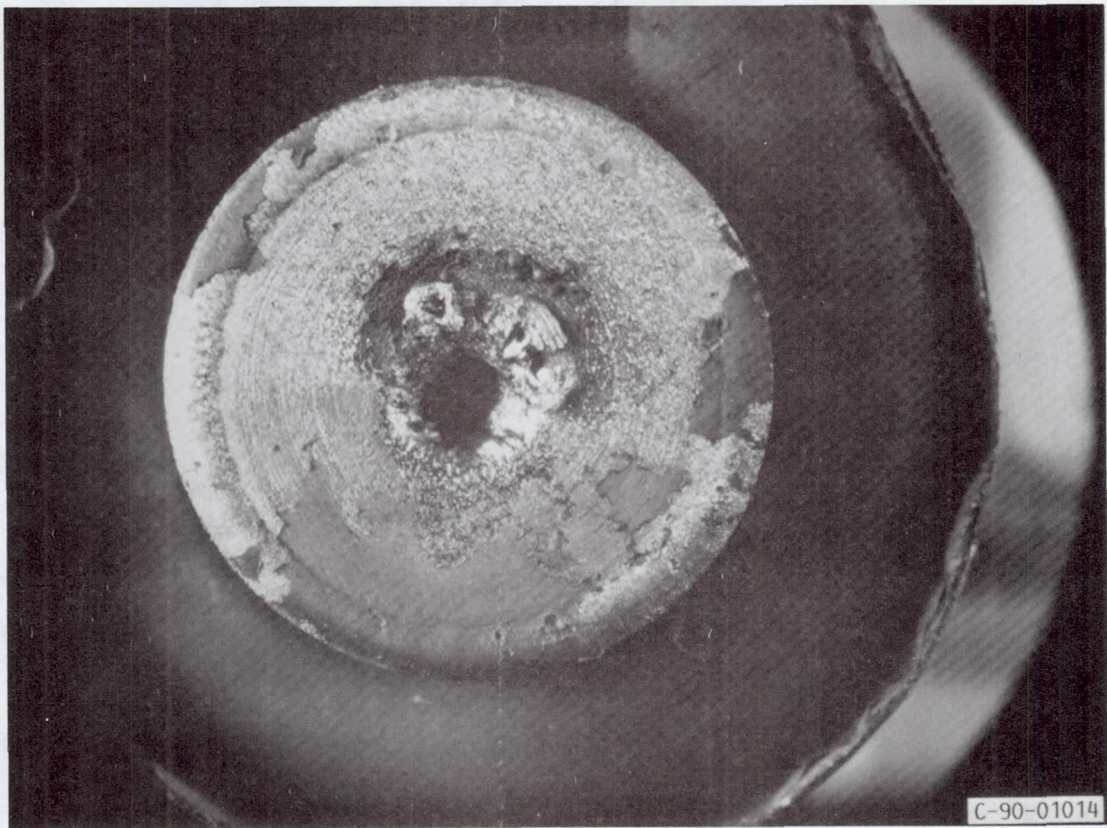
(B)   Post-Lifetest.
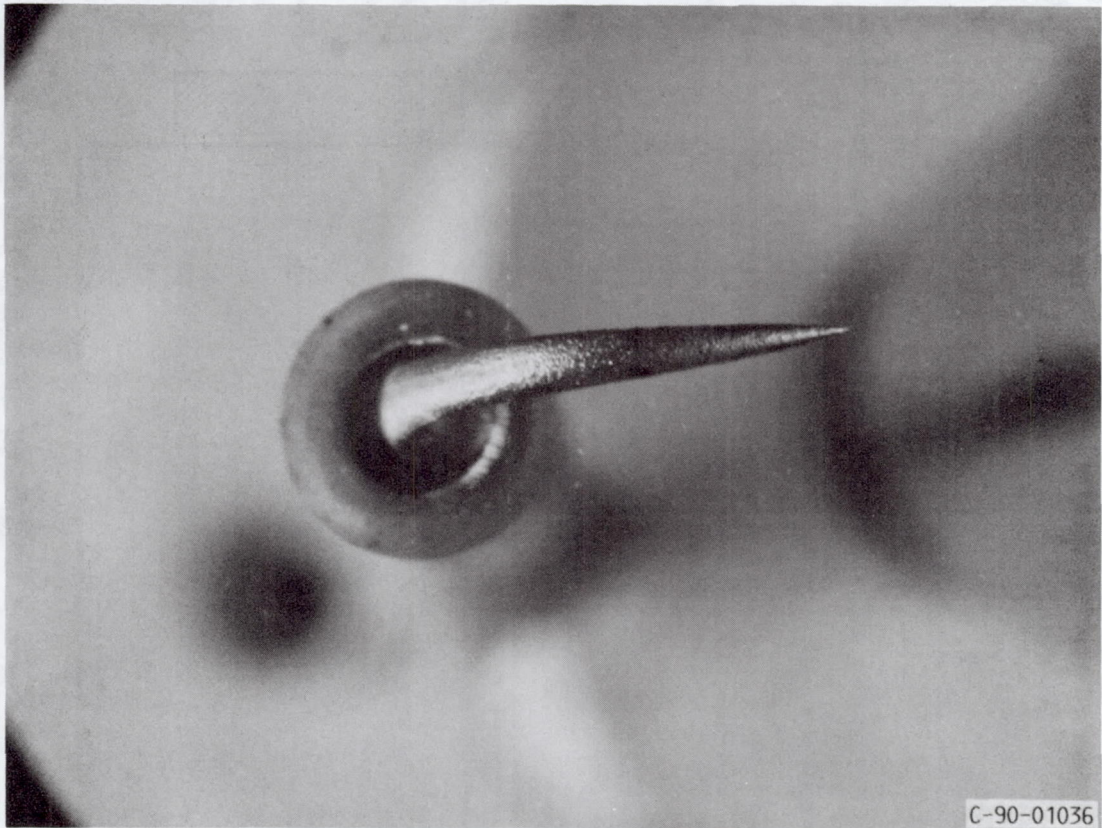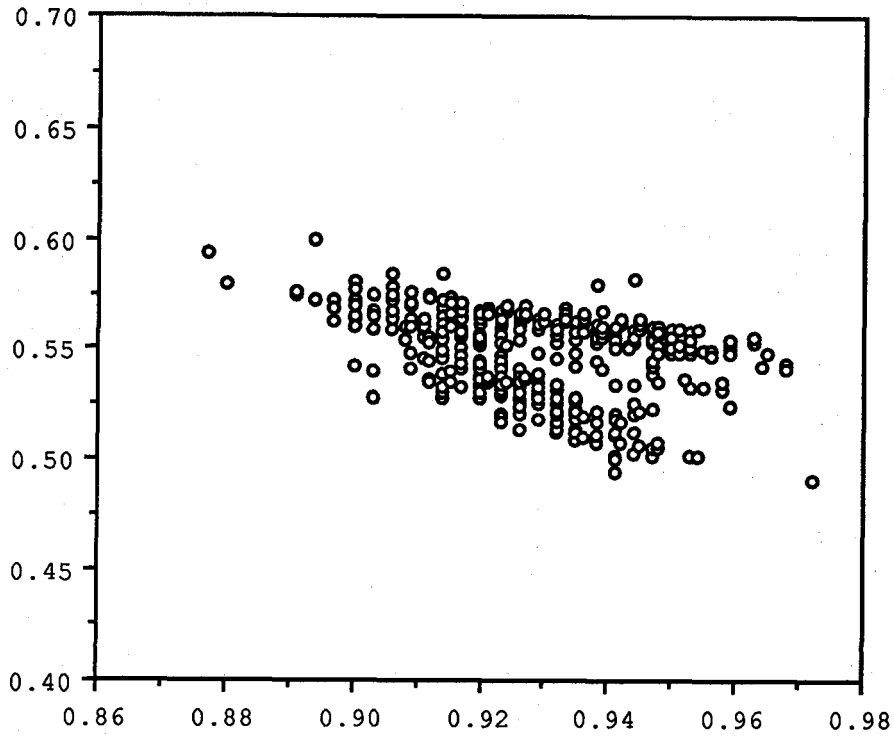

FIGURE 37. - Neutralizer Cathode Orifice Plate.
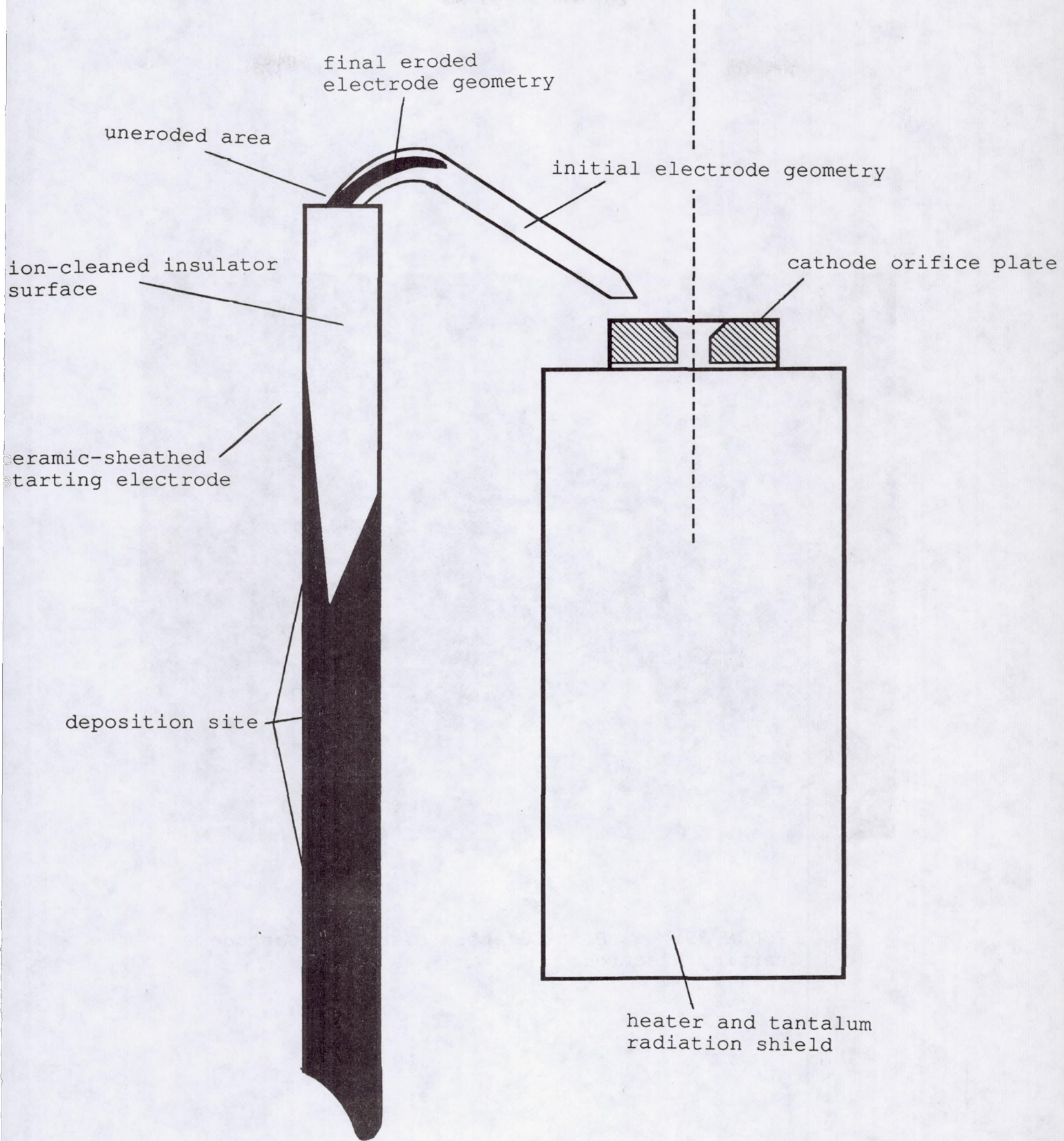
FIGURE 38. — Discharge Cathode Starting Electrode Geometry, Pre- and Post-Lifetest.

FIGURE 39. - Post-Lifetest Discharge Cathode Starting Electrode.

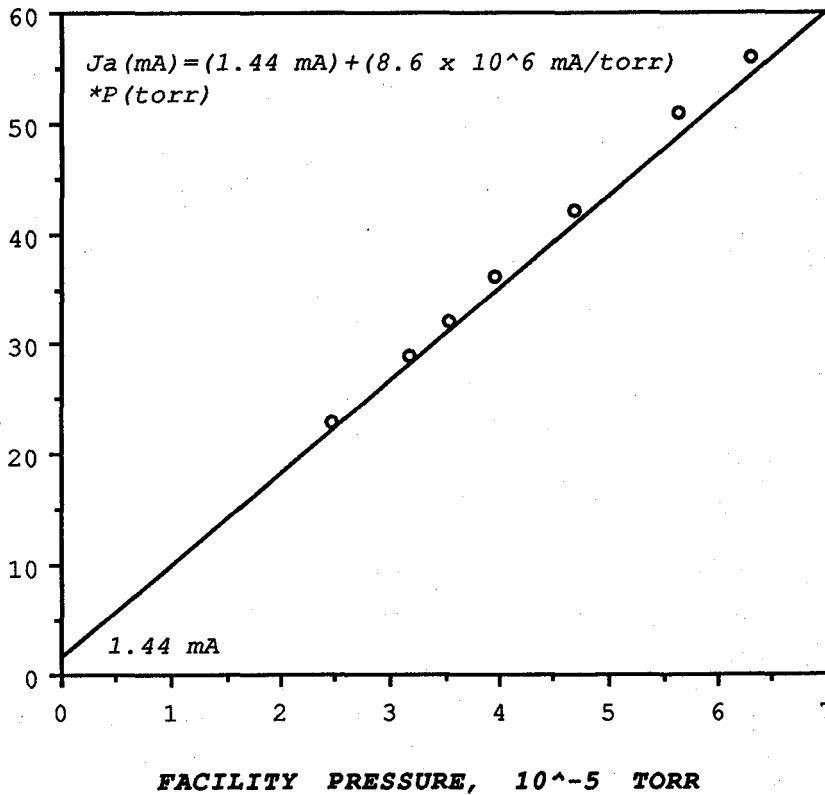FIGURE 40. - Ratio of Ja/Jb versus
Discharge Propellant Efficiency,
for Lifetest Duration.

$Ja(mA) = (1.44\ mA) + (8.6 \times 10^6\ mA/torr) *P(torr)$

1.44 mA

FACILITY PRESSURE, 10^{-5} TORR

FIGURE 41. - Sensitivity of Accelerator Grid
Impingement Current to Facility Pressure.

Report Documentation Page

1. Report No. NASA TM-103191 AIAA-90-2543	2. Government Accession No.	3. Recipient's Catalog No.

4. Title and Subtitle		5. Report Date
5-kW Xenon Ion Thruster Lifetest		
		6. Performing Organization Code

7. Author(s)	8. Performing Organization Report No.
Michael J. Patterson and Timothy R. Verhey	E-5579
	10. Work Unit No. 506-42-31

9. Performing Organization Name and Address	11. Contract or Grant No.
National Aeronautics and Space Administration Lewis Research Center Cleveland, Ohio 44135-3191	
	13. Type of Report and Period Covered Technical Memorandum

12. Sponsoring Agency Name and Address	
National Aeronautics and Space Administration Washington, D.C. 20546-0001	14. Sponsoring Agency Code

15. Supplementary Notes

16. Abstract

This paper describes the results of the first lifetest of a high power ring-cusp ion thruster. A 30-cm laboratory model thruster was operated steady-state at a nominal beam power of 5kW on xenon propellant for approximately 900 hours. This test was conducted to identify life-limiting erosion modifications, and to demonstrate operation using simplified power processing. The results from this test are described including the conclusions derived from extensive post-test analyses of the thruster. Modifications to the thruster and ground support equipment, which have been incorporated to solve problems identified by the lifetest, are also described.

17. Key Words (Suggested by Author(s))	18. Distribution Statement
Ion propulsion Electric propulsion Lifetest Xenon ion	Unclassified – Unlimited Subject Category 20

19. Security Classif. (of this report)	20. Security Classif. (of this page)	21. No. of pages	22. Price*
Unclassified	Unclassified	52	A04